



Aalto University  
School of Electrical  
Engineering

AALTO UNIVERSITY  
SCHOOL OF ELECTRICAL ENGINEERING

Department of Electrical Engineering and Automation

**Jay Panchal**

## **3 DIMENSIONAL ELECTROMAGNETIC ANALYSIS OF AN AXIAL ACTIVE MAGNETIC BEARING**

**Thesis supervisor:**

**Professor Anouar Belahcen**

**Thesis Advisor:**

**Dr. Erkki Lantto (Sulzer Pumps Finland Oy.)**

Author : Jay Panchal		
Title : 3 Dimensional Electromagnetic Analysis of an Axial Active Magnetic Bearing		
Date: 21.07.2016	Language: English	Number of pages: 7 + 74
Department of Electrical Engineering and Automation		
Professorship: Electromechanics		Code: S-17
Supervisor: Professor Anouar Belahcen		
Advisor: Dr. Erkki Lantto		
<b>ABSTRACT</b>		
<p>In the rotating electrical machines, active magnetic bearing are basically performing the same role like mechanical bearings to support rotor. The function is based on the principle of magnetic levitation. The idea behind this involves creation of a magnetic field by supplying controlled currents in the bearing coil through amplifiers and complex power electronics. The accurate design of a magnetic bearing system incorporates many parameters before its implementation. The current work of the thesis encircles only the three dimensional (3D) modeling of axial active magnetic bearing (AMB). The static and dynamic models are analyzed for the bearing with a consideration of nonlinear material. In the study, the major emphasis is on the magnetic field, eddy current behavior and exerted magnetic forces in the magnetic bearing. The required input parameters for simulation are considered from the available two dimensional (2D) analysis for the same axial actuator. Elmer open source finite element tool is used in the entire work for making 3D simulations. Finally, the computed results are compared with the 2D case. As a part of the thesis work, a modified geometry is simulated to analyze eddy currents. The hypothesis in later task is the reduction of eddy current losses by providing a radial cut in the bearing ferromagnetic path. The radial cut brings asymmetry in the bearing and the three dimensional analysis provides the possibility to analyze the complete model. The results obtained in the above work provide a good understanding of 3D fields in axial AMB and the computed magnetic forces are in good agreement with the 2D results.</p>		
Keywords: Active Magnetic Bearing(AMB), Finite Element Method (FEM), Eddy Currents, Magnetic Force		

## **ACKNOWLEDGEMENTS**

This master's thesis is part of the SEMTEC project which is partially funded by Tekes - the Finnish Funding Agency for Innovation. The thesis work was jointly carried out at Sulzer Pumps Finland Oy and Aalto University, Finland in the Department of Electrical Engineering and Automation. I would first like to thank my supervisor Prof. Anouar Belahcen for providing me the opportunity to work in his research group. His motivation and guidance helped me to learn a lot from this project and make my fundamentals stronger. The thesis could not have been successfully completed without active guidance and encouragement of my advisor Dr. Erkki Lantto. He has always been generous in resolving my doubts and many times stayed back till late after his office hours for helping me. I would like to convey special thanks to Mr. Ville Tommila who has been a great support during thesis work. The discussions with him has helped me in getting out of many problems and also developed detail understanding of AMB system. I would like to thank Dr.Artru Reunanen for providing me an opportunity to be a part of Sulzer Pumps Solutions Finland Oy. I convey my gratitude to all other colleagues at Sulzer Pumps who have helped me in numerous ways and provided me an excellent and enjoyable work environment. My tenure at Electromechanics department of Aalto University was always supported with endless help of colleagues. I want to thank Dr. Vicente, Dr. Floran, Sabin, Antti, Bishal, Sahas, Victor and all other staff who imparted their valuable time for resolving my doubts. I am obliged to Mr. Ari Haavisto for arranging all required technical resources during my work. Thanks are also extended to Peter Råback, Juhani Kataja and Mika Malinen from CSC-IT center for science, Finland. Their continuous support helped me to develop good skills with Elmer FEM tool and attain success in using new features of Elmer. I would also like to acknowledge all members of SEMTEC group for useful discussions during meetings. Those discussions were very useful for me in getting good start of work.

Most of all, I thank my parents and sister for providing me moral support during this challenging journey. I thank Ravi for being helpful during and after his work hours. I am also thankful to all my friends at Aalto University for providing the most memorable and enjoyable time of my life.

# TABLE OF CONTENTS

<b>ABSTRACT .....</b>	i
<b>ACKNOWLEDGEMENTS.....</b>	ii
<b>TABLE OF CONTENTS.....</b>	iii
<b>LIST OF SYMBOLS AND ABBREVIATIONS.....</b>	v
<b>1. INTRODUCTION.....</b>	1
1.1 BACKGROUND.....	1
1.2 GENERAL DETAILS OF CONSTRUCTION AND OPERATION .....	1
1.3 AIM OF THE THESIS.....	4
1.4 SCIENTIFIC CONTRIBUTION OF THE WORK .....	5
1.5 STRUCTURE OF THESIS.....	5
<b>2. LITERATURE REVIEW AND METHODOLOGY .....</b>	6
2.1 ACTIVE MAGNETIC BEARING .....	6
2.1.1 Force.....	6
2.1.2 Power Losses.....	8
2.1.3 Computational Technique .....	10
2.2 MAXWELL'S EQUATIONS .....	10
2.2.1 Integral form of Maxwell equations.....	11
2.3 FINITE ELEMENT METHOD .....	12
2.3.1 Nodal Element.....	14
2.3.2 Edge Element .....	14
2.4 EDDY CURRENT FORMULATIONS .....	16
2.4.1 AV-A Formulation .....	17
2.4.2 Eddy Current Solutions with application of Edge Element through Elmer .....	18
2.5 MAGNETIC FORCE EVALUATION .....	19
2.6 METHODOLOGY .....	22
<b>3. STATIC MODEL.....</b>	23
3.1 OVER VIEW OF MODEL .....	23
3.1.1 Construction .....	23
3.1.2 Mesh.....	24
3.2 MODEL PARAMETERS .....	26

3.2.1 Boundary Condition .....	26
3.2.2 Parameters .....	27
3.3 Results and Observations .....	28
<b>4. DYNAMIC MODEL</b> .....	35
4.1 MODEL PARAMETERS .....	35
4.2 TIME STEPPING: .....	36
4.3 HIGH AMPLITUDE SIMULATIONS.....	36
4.3.1 Eddy current and Flux Density Distribution .....	36
4.3.2 Magnetic Force evaluation with Elmer simulations.....	42
4.3.3 Eddy Current Loss and Paraview Results .....	45
4.3.4 Simulation Time.....	45
4.4 MODIFIED DESIGN.....	46
4.5 MODELING OF THE SHAFT ROTATION.....	47
<b>5. CONCLUSION AND DISCUSSION</b> .....	49
<b>6. FUTURE WORK</b> .....	51
<b>APPENDIX I MAGNETIZING PROPERTY</b> .....	52
<b>APPENDIX III RESULTS FOR LOWER MESH DENSITY</b> .....	55
<b>APPENDIX IV ELMER SIMULATION CODE</b> .....	58
<b>APPENDIX V PENETRATION DEPTH</b> .....	70
<b>REFERENCES</b> .....	72

# LIST OF SYMBOLS AND ABBREVIATIONS

$a$	Index for solution at specified time step in BDF method
$A$	Magnetic vector potential
$A_a$	Cross sectional area in air gap
$A_{fe}$	Cross sectional area in iron
$B$	Magnetic flux density
$B_{air}$	Magnetic flux density in air
$B_m$	Maximum magnetic flux density
$d$	Surface thickness
$D$	Electric flux density
$E$	Electric field strength
$F$	Magnetic force
$F$	Function assign for spatial coordinate and time
$f_s$	Supply frequency
$f_r$	Frequency of flux reversal
$h$	Skin depth penetration factor
$H$	Magnetic field strength
$i$	Node index
$I$	Magnitude of coil current
$j$	Node index
$J$	Current density
$J_M$	Jacobian matrix
$K_{e\_classic}$	Eddy current Coefficient
$K_h$	Material constant for hysteresis loss
$k$	Time step number
$L$	Lagrange polynomial
$M$	Discretized Identity operator
$n$	Number of turns in the coil

$N$	Shape function
$P_e$	Eddy current loss
$P_h$	Hysteresis Loss
$R$	Resistance of Coil
$S$	Differential operator
$\mathbf{T}$	Electric vector potential
$U$	Nodal electric potential
$v$	Reluctivity of material, Velocity of charge particle in Lorentz force equation
$V_{fe}$	Volume of iron
$V$	Electric scalar Potential
$\mathcal{V}$	Volume of domain under integration in magnetic force equation
$W$	Magnetic Energy in the system
$W_g$	Magnetic Energy in the air gap
$\lambda$	Thickness to skin depth ratio
$\Lambda$	Area coordinate of node
$\rho$	Electric charge density
$\mu$	Permeability of material
$\mu_0$	Permeability of air
$\mu_r$	Relative Permeability of material
$\sigma$	Electrical conductivity of material
$\varepsilon$	Electrical permittivity
$\delta$	Air Gap length
$\Omega_1$	Eddy current region
$\Omega_2$	Eddy currents free region

## **Abbreviations**

2D	Two Dimensional
3D	Three Dimensional
AC	Alternating Current
AMB	Active Magnetic Bearing
DC	Direct Current
FEM	Finite Element Method
FEA	Finite Element Analysis

# CHAPTER 1

## INTRODUCTION

This introductory chapter is segregated into three different sections. The first part contains a brief overview and history of Active Magnetic Bearing (AMB) systems. In subsequent section the working principle of active bearing arrangements and their constructional details are explained. The benefits and disadvantages of AMB are highlighted in the same section. In the later part, the targets of the entire thesis work are discussed. Subsequently, at the end the scientific outcome of the work and the structure of thesis text are enumerated.

### 1.1 BACKGROUND

The concept of magnetic levitation has been researched over more than a century. In 1842, the English mathematician, Samuel Earnshaw was the first one to introduce this idea with the electrostatic field (later referred to magnetic field also) and proved it to be an impossible feature. But Emile Bachelet implemented Earnshaw's theorem and patented the concept of levitating transmitting apparatus in 1912, while Herman Kemper followed him by achieving a patent in 1937 for his invention of the electromagnetic suspension for tracked vehicle. Kemper's idea became popular in MAGLEV trains (Schweitzer *et al.*, 2009). These past work on the idea of levitation by scientists of different era, have also resulted in the evolution of magnetic bearings, which efficiently substituted the mechanical bearing concept.

The bearings are the essential part of all type of rotating machines, as they support and ensure the position of rotational axis. As far as the application and construction are concerned, bearings can be classified in many categories. Since few decades magnetic bearings are intensely gaining popularity among research engineers. They are more attractive due to their contactless function, which makes them free from lubricants, friction and mechanical wears. Since the entire function is based on levitation, magnetic bearings offers higher immunity to temperatures changes, robust operation and extended limits for rotational speed. In addition to the above benefits, active magnetic bearings provide possibilities of having excellent vibration control and active compensations for an unbalanced rotor.

### 1.2 GENERAL DETAILS OF CONSTRUCTION AND OPERATION

As introduced in the preceding section, the forces in magnetic bearing are created electromagnetically with the help of actively controlled currents. The operating principle of AMBs offers room for implementing novel ways to deal with problems of rotor dynamics.

According to the direction of the applied force with respect to the shaft axis, magnetic bearings can be classified as axial and radial magnetic bearing. As the names indicate, radial bearing controls radial movements while axial bearing takes care of axial offsets of the rotor. Figure 1.1 shows the basic structures for both bearings. Radial bearing consist of projected poles with a winding over them and they create force of attraction on the rotor in four directions orthogonal to the rotor axis. The axial bearing consists of an actuator with a coil housing in the stator and a disc shaped rotor section. The construction is axially symmetric in the later.

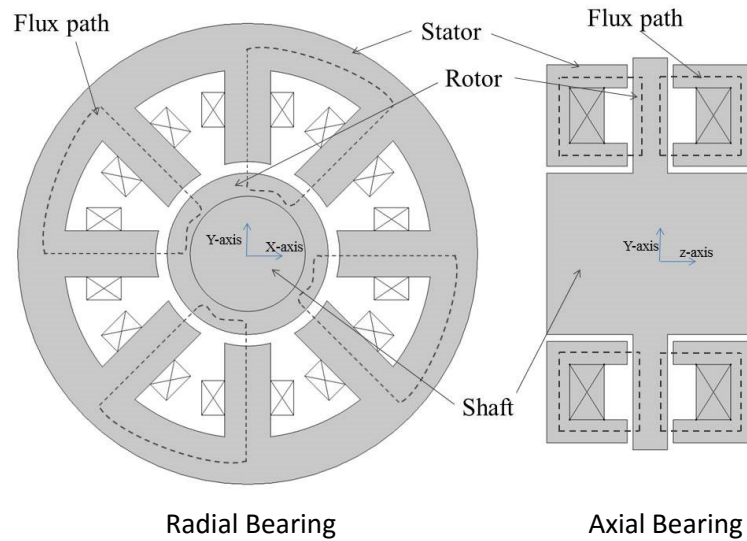
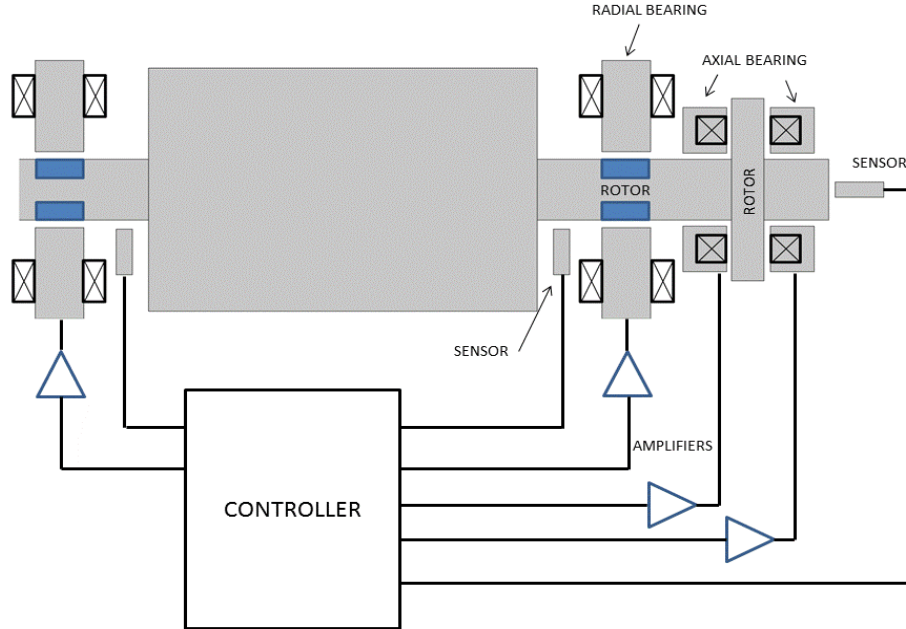


Figure 1.1 Radial eight-pole magnetic bearing and axial disc-type bearing

Till some extent, the electrical motors and magnetic bearings have fundamental resemblance. As in later the magnetic actuator being constructed from soft ferromagnetic material and is electromagnetically activated by copper windings. This generates attractive force in the air gap between the stators and the shaft.

Magnetic bearing systems can be divided into four basic components: (1) magnetic actuator; (2) Control system; (3) power amplifier; (4) shaft position sensor; (5) UPS (Uninterruptable Power Supply) (Lantto, 1999) (R. Gouws, 2004). Each component plays an essential role in achieving accurate levitation.



*Figure 1.2 Arrangement of radial and axial magnetic bearing on the shaft of the motor*

As shown in Figure 1.2 the coils of the bearing unit are supplied with controlled current through a power amplifier. The magnitude of the current supplied to coil is precisely controlled with a PWM controller. The main task of the controller is to maintain the rotor position at predefined coordinates. The decisions made by the controller are based on the rotor position data, which is continuously measured by contact-less (eddy current, inductive or capacitive) position sensors. The deviation with respect to desired position is sensed both in radial and axial directions. The rotor suspended with the combination shown in Figure 1.2, will have position control in five degrees of freedom. In such configuration, the rotating shaft can solely be supported by the magnetic fields. With the magnetic bearing the rotation of the shaft can be boosted beyond 200m/s of surface speeds (Knospe *et al.*, 1997) (Lantto, 1999). The speed constraint is subject to limits of stress due to centrifugal forces. The magnitude of stress depends on the shape, dimensions and the material of the rotor (Knospe *et al.*, 1997). This concept is thoroughly explained by Laronneur (1990). Although magnetic bearings show high reliability in normal operations, there are limitations faced due to their low mechanical stiffness during faults. The levitation ceases during emergency power breaks and to ensure safe run down of rotor touch down bearings are needed (Carmignani *et al.*, 2001). These secondary bearings are the conventional mechanical bearings, which also support the rotor during stand still condition. The inner diameter of the mechanical bearing is deliberately kept smaller compare to the radial airgap between the magnetic bearing and the shaft (Lantto, 1999).

The magnetic bearing technology finds immense application in pumps, turbo-compressors, milling spindles and turbo-molecular pumps. Magnetic bearings can work in vacuum with

zero friction loss, which make them an ideal choice for applications like space vehicles and fly wheel storage. A proper design of an AMB system, can work efficiently years long, and the designer needs equal knowledge of multiple area viz. control, electronics and electro-mechanics (Lantto, 1999). Due to the complex structure of AMB systems, they are considered expensive in comparison with conventional lubricated bearings (Betschon, 2000). Despite the higher cost, AMBs have shown numerous functional advantages, which have increased their applications.

### 1.3 AIM OF THE THESIS

The industries are rigorously advancing towards high speed machines because of recent developments in ultra-high speed drives with high power density. Such high speed operation can be facilitated by the use of AMBs, which make them ideal choice for industries. The rotor at such high speed requires more precision in control and faster dynamics of bearing. The force response which is considered as one of the key features for AMB, can be improved with proper control schemes. The difficulties in attaining high dynamics are faced due to the high eddy currents in the conducting region of the magnetic circuit. The eddy current fields cause phase lag between the coil current and the magnetic forces, which increases with the increase in eddy currents. This problem needs to be handled by making proper design of the magnetic circuit. The eddy current loss analysis in the design stage calls for diligent study of the fields in the actuator beforehand. There are detailed studies made for actuator fields by engineers in the past using analytical techniques. However owing to the requirement of higher accuracy, the FEM is becoming a popular choice. Since few decades the FEM is the most preferred method by scientists and engineers for solving such problems in electromagnetic domain. The present thesis work is focused on the use of the FEM technique with Elmer, an open source software tool, for analyzing the complete actuator of an axial magnetic bearing in 3D. Nearly half portion of the work in the present thesis is focused on the eddy current loss study and modeling. The remaining part of the work is carried out on the force analysis with the help of the generalized nodal forces approach. Considering the axis symmetry of the axial actuator of the AMB under investigation, it has been analyzed first with a 2D approach. However some limitations are faced when it comes to the modeling of asymmetries in the system. 3-D modeling suits best for this work, as the asymmetry can be defined in the problem. The eddy current magnitude can be reduced to a lower value by breaking their circulation path, and at the same time not hampering the flux path. This study is part of later stage of this thesis which deals with the modification of the initial design.

The target of thesis was limited to the analysis of an axial bearing, hence the radial bearing shall be out of the analytical discussion. However one can find detailed analysis of the design and control of radial bearing in the work of Schweitzer et al. (2009), Lantto (1999), Betschon (2000) and (Knospe et al., 1997).

## **1.4 SCIENTIFIC CONTRIBUTION OF THE WORK**

The present work of thesis is based on the development of a method to analyze axial active magnetic bearing in 3D. At present, the actuator is axially symmetric, hence the 2D FEM approach is a convenient way of analysis. However, a radial cut in the bearing magnetic circuit creates asymmetry in the geometry, which cannot be modeled in 2D FEM. The thesis provides the idea of simulating the complete 3D model of the actuator in an open source multiphysical simulation software, Elmer. The tool is developed by CSC-IT center for science, Finland.

The defined method is also proposed for further work with cut geometry. The major part of the work covers comparative studies of the results obtained in 3D and 2D cases for magnetic force values, eddy current power loss, eddy current densities and Flux densities.

## **1.5 STRUCTURE OF THESIS**

For encrypting the work done and achieved targets, the thesis is divided into several chapters. The chapter 2 provides general background and theoretical understanding of losses and their force analysis in magnetic bearing. The information reviewed from several literatures is synthesized in the same chapter. The basic theory of FEM and various formulations concerning to eddy current and magnetic forces are also explained in that chapter. In the chapter 3, the steady simulation results with DC current input to the coil of actuator are presented and explained. The chapter includes brief details of considered boundary conditions in problem domain. The light is also shaded on meshing of model and its technicalities. The chapter 4 gives details about time stepped simulation results. This chapter contains core information about thesis work and provides understating of obtained 3D FEM results in comparison to reference 2D FEM. The discussion encircles the eddy current, the flux density distribution and the magnetic forces in the studied axial actuator. The modified design is also explained in same chapter. In the Chapter 5 concluding remarks and brief summary about the work done are presented. The future work is proposed in the chapter 6.

# CHAPTER 2

## LITERATURE REVIEW AND METHODOLOGY

### 2.1 ACTIVE MAGNETIC BEARING

In the previous chapter, Figure 1.2 illustrated the operation layout of the AMB along with its basic components. The working principle of the AMB is based on magnetism (Gouws, 2004). The magnetic actuator of the radial bearing comprises of attractive electromagnets, which are arranged around a magnetically permeable cylinder attached to the shaft. The attractive force generated by the electromagnets is used to support a rotating shaft. For measuring x and y positional offsets, position sensors are provided, which are generally placed along the shaft, right after the actuator. The position signal is continuously produced by those measurements and controller computes the requested coil current. Without any control system, the bearing with such a concept of electromagnet is unstable as the attractive force increase with the decrease in the distance of the rotor from the electromagnets. The controller receives position error data and modifies the magnitude of coil currents accordingly. The coil current will be increased for the poles opposite to the displacement direction and reduced for the poles in the direction of displacement. This action produces a restoring force which tends to stabilize the system.

The radial bearing takes care of 4 degrees of freedom:  $x_1$ ,  $y_1$ ,  $x_2$  and  $y_2$ , while the axial bearing will retain the shaft position in the z (axial) direction. Fundamentally, the axial bearing works in quite similar way as discussed above but only in only axial direction. Hence relatively their control is easier compare to radial bearing.

Before designing AMBs for a specific practical application, there are certain aspects to be taken into consideration viz. load, size, stiffness, temperature, precision, speed, losses and dynamics. Even the complex issues like reliability and smartness of the bearing can be seen as features with increasing importance and growing maturity (Schweitzer, 2002).

#### 2.1.1 Force

The loading capacity of AMBs depends on the arrangement and geometry of the electromagnets, the magnetic properties of material, the amplifier (power electronics) and the art of control implemented. The external forces on AMBs are not static but dynamic in nature. Under static loading, the force exerted by the axial actuator in Figure 1.1 can be realized through a simple geometrical structure as shown in figure 2.1 below.

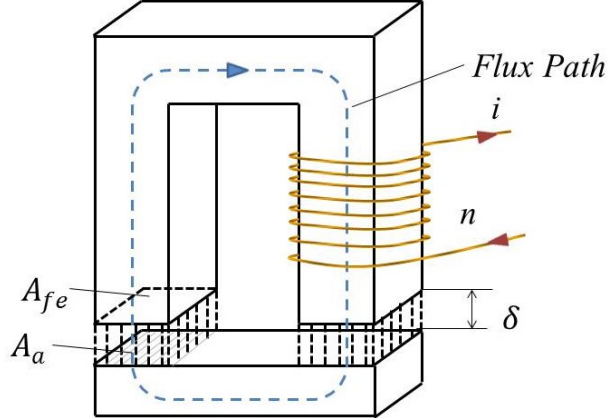


Figure 2.1 Axial actuator Realized as Electromagnet

The magnetic field, which is responsible for magnetic forces, is generated by the coil current  $I$ . If the coil is supposed to have  $n$  turns, then the integration path for the magnetic field strength  $\mathbf{H}$  covers several current loops and the integral for of Ampere's law yield the magnetomotive force

$$\bigcirc \mathbf{H} \quad (2.1)$$

The fundamental relation between the magnetic flux density  $\mathbf{B}$  and  $\mathbf{H}$  is

$$\mathbf{B} = \mu_0 \mu_r \mathbf{H} \quad (2.2)$$

where  $\mu_r$  is the relative magnetic permeability

For the ferromagnetic material used in the iron parts,  $\mu_r \gg 1$  and the saturation limits are defined by those portions of the magnetic circuit. The force expression is defined by considering the actuator operation in linear region and at low frequency. This makes the flux density uniform in the airgap and iron parts. The energy stored in the two air gaps can be given by

$$W_g = \frac{1}{2} B_{air} H A_a 2\delta \quad (2.3)$$

Based on virtual work principle and constant flux, the expression for magnetic force is given by

$$F = -\frac{\partial W_g}{\partial \delta} = -B_{air} H A_a \quad (2.4)$$

$$F = -\mu_0 A_a \left( \frac{nI}{2\delta} \right)^2 = -\frac{1}{4} \mu_0 n^2 A_a \left( \frac{I}{\delta} \right)^2 \quad (2.5)$$

The maximum force is limited by the allowable magneto motive force,  $n \cdot I_{\max}$ . The maximum current  $I_{\max}$  is decided on the basis of temperature limits and the second limit is faced at the saturation point of iron. The power source should also be capable enough to reach that maximum limit of the current.

### 2.1.2 Power Losses

In AMB system, the achievable AMB force slew rate has implications of amplifier voltage limits (Yang, 1997). Generally the current in the coils is operated around a bias level so as to have a significant force slew capability when there is no net force (Knospe et al., 1997). However, a drawback with bias level operation is seen in case of the radial bearings. The rotor faces frequent flux change leading to high eddy currents. The associated hysteresis losses also increase under such operation. For high speed rotating machinery, these losses may result in excessive rotor heating, hence the rotor is always kept laminated in the case of radial bearing. The stator is also usually laminated to reduce eddy currents caused by flux changes.

In case of axial bearing, since the structure is symmetric around the axis, there are no eddy currents induced by rotation. But still there are eddy current power loss due to varying flux and the major part of it is observed in the stator. The figure 2.2 gives good realization of induced eddy current.

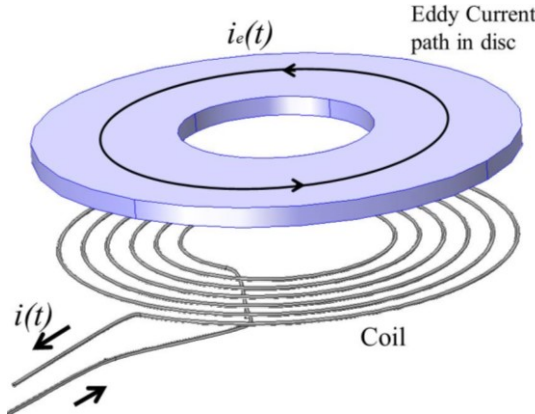


Figure 2.2 Induced eddy current in a disc exposed to the time varying field of a coil

The eddy-current losses ( $P_e$ ) can be reduced by dividing the iron core in insulated sheets, or in particles (sinter cores). The smaller these divisions are the less will be the eddy-current losses. The rotor part in axial magnetic bearing is a disc and it has to face high centrifugal force, hence it is usually made of solid iron. The stator is also usually constructed from solid iron. The losses in the iron can be analytically calculated by a classical approach (Schweitzer, 2002) (Popescu, 2007).

$$P_e = K_{e\_classic} f_r^2 B_m^2 V_{fe} \quad (2.6)$$

Here  $f_r$  is re-magnetization frequency,  $B_m$  is maximum flux density in iron,  $V_{fe}$  is the volume of iron and  $K_{e\_classic}$  is the eddy current coefficient, which is expressed as

$$K_{e\_classic} = \frac{\pi^2 d^2}{6\rho} \quad (2.7)$$

Where  $d$  is the thickness of the surface where the eddy current enters orthogonally and  $\rho$  is the specific resistance of the material.

The work of Mayergoys *et. al* (1984), explains the physical phenomenon of the field penetration into a ferromagnetic material and its importance. The skin depth penetration is one of the factors to be considered and it can be given by:

$$h = \sqrt{\frac{\rho}{\pi f_r \mu}} \quad (2.8)$$

It give the measure of the distance where the field is decreased by a ratio of 1/e (approx. 37%)

The eddy current coefficient varies as per frequency after imposing effect of skin depth. The final expression can be give as (Popescu, 2007)

$$K_e(f_r) = \frac{\pi^2 d^2}{2\rho\lambda} \cdot \frac{\sinh \lambda - \sin \lambda}{\cosh \lambda - \cos \lambda} \quad (2.9)$$

$$\text{Where, } \lambda = \frac{d}{h}$$

Besides the eddy current losses, the hysteresis losses  $P_h$  are also part of the core losses. They are caused by the fact that the magnetization follows hysteresis loop instead of single-valued B-H curve during a periodic excitation. The hysteresis losses can be given by (Popescu, 2007)

$$P_h = K_h f_r B_m^{1.6} V_{fe} \quad (2.10)$$

where,  $K_h$  is a material constant derived from loss measurements and the area of the hysteresis loop.

For high speed rotating machinery, the eddy current losses are dominating, and the hysteresis losses have marginal percentage share of the total losses. Hence, the accuracy is not much affected if the hysteresis is neglected for high speed operations. Also eddy currents are a more essential part of the study in AMB design as they produce unpredicted forces, which can lead to a malfunction of the magnetic bearing. The scenario is different in low speed operation, as hysteresis shares a major portion of the total core losses (Hull, 1995), which then needs to be modeled. The current thesis is not extended to model the hysteresis loss, as it is dealing with eddy current analysis. One can find method of evaluating hysteresis loss from the past work of Meeker *et. al.* (2004) in magnetic bearings.

### **2.1.3 Computational Technique**

The magnetic circuit in axial AMBs is quite simple and for linear operation zone, the magnetic force shows linear dependence on the square of the magnetic flux density. The flux density itself is linearly related to the current. For modeling the actuator under such situation, many times analytical expressions are used to get a preliminary idea of the force and the average flux density. For getting highly accurate results, the most favorable approach is the Finite Element Analysis (FEA) as proposed by Antila(1998) and Lantto (1999).

During the 1950s, the FEM was only applied to structural analysis, mechanics and aeronautical field of studies. But after 1970, FEM found application in electromagnetics, which made irregular domains possible to be analyzed (Mason, 1982). J L Mason (1982) analyzed scattered electromagnetic field with unbounded space in (Mason, 1982) using 2D FEM. The technique was more promising for engineers in electromagnetics, as it was able to model nonlinearities in the material. Computationally, FEM can be an expensive approach, due to which in early years, 3D FEM was not explored much. Instead it was reduced to 2D model for further evaluations. With increased maturity level of computation, nowadays, engineers and scientists are encouraged to solve complex 3D model using FEA (Arkkio, 1987). The analytical or numerical methods can be useful for making preliminary estimates as they can provide quick solution.

## **2.2 MAXWELL'S EQUATIONS**

The magnetic problems are solved with steady state equations unless there are time varying magnetic fields. Such fields, when they are present in the problem domain give rise to an electric field, which is also true the other way around. The electromagnetic (EM) fields and therefore, eddy currents can also be expressed using Maxwell's Equations. The equations are used in quasi-static form for analyzing the magnetic field problems. Following are the fundamental differential forms (EM quantities), which are considered as the starting point of FEM for electro magnetics.

Ampere Law states that the magnetic field  $\mathbf{H}$  is formed in orthogonal plane around any conductor carrying current with current density  $\mathbf{J}$ .

$$\nabla \times \mathbf{H} = \mathbf{J} + \frac{\partial \mathbf{D}}{\partial t} \quad (2.11)$$

The above equation is generally referred to as the Ampere's law with Maxwell's correction. Where,  $\partial \mathbf{D} / \partial t$  is the time varying electric flux density added by Maxwell. But the problem domain that we work with is quasi-static, so in that case electric flux is constant or  $\partial \mathbf{D} / \partial t$  very small compare to  $\mathbf{J}$ . Hence the expression is reduced to:

$$\nabla \times \mathbf{H} = \mathbf{J} \quad (2.12)$$

The magnetic flux follows a law of conservation. The flux entering into a volume is equal to the flux leaving out of the volume. Hence mathematically the divergence of the flux density is zero

$$\nabla \cdot \mathbf{B} = 0 \quad (2.13)$$

The magnetic flux density changing with respect to time generates electric field intensity  $\mathbf{E}$  and can be expressed as

$$\nabla \times \mathbf{E} = -\frac{\partial \mathbf{B}}{\partial t} \quad (2.14)$$

Unlike the magnetic flux, the electrical field has monopoles, hence the electric flux  $\mathbf{D}$  is not conservative. The electric flux entering a volume is not equal to the electric flux leaving out. This phenomenon can be well understood by considering a point charge  $q$  enclosed by a sphere. The point charge will produce the flux lines oriented outwards from the surface (Bastos, 2003). Thus the electric charge density  $\rho$  seen inside the volume is given by the divergence of electric flux density  $\mathbf{D}$ .

$$\nabla \cdot \mathbf{D} = \rho \quad (2.15)$$

### 2.2.1 Integral form of Maxwell equations

The application of Maxwell equation can be generalized when they are used in integral form. In all kind of electro-mechanical problems, at some point, Maxwell equations are applied in integral form (Bastos, 2003). Applying stokes theorem to the integral form of (2.12), the resulting equations are:

$$\oint \mathbf{H} \cdot d\mathbf{s} = \int \mathbf{J} \cdot ds \quad (2.16)$$

$$\int_{L(S)} \mathbf{H} \cdot d\mathbf{s} = \int_S \mathbf{J} \cdot ds \quad (2.17)$$

Applying the same to equation (2.14), one obtains (Bastos, 2003)

$$\int_s \nabla \times \mathbf{E} \cdot ds = - \int_s \frac{\partial \mathbf{B}}{\partial t} \cdot ds \quad (2.18)$$

$$\circ \quad \mathbf{E} \quad \frac{\partial \mathbf{B}}{\partial t} \cdot ds \quad (2.19)$$

Using Gauss theorem for the magnetic flux density and Electrical Flux density in equation (2.13) and (2.15) respectively, we end up at following equations (Bastos, 2003)

$$\circ \quad \mathbf{B} \quad (2.20)$$

$$\circ \quad \mathbf{D} \quad \circ \quad (2.21)$$

The variables in the equations above are related to each other by a set of constitutive relations. Those relations describe different properties of the material and the medium in which the material is placed. The constitutive laws can be expressed as:

$$\mathbf{B} = \mu \mathbf{H} \quad (2.22)$$

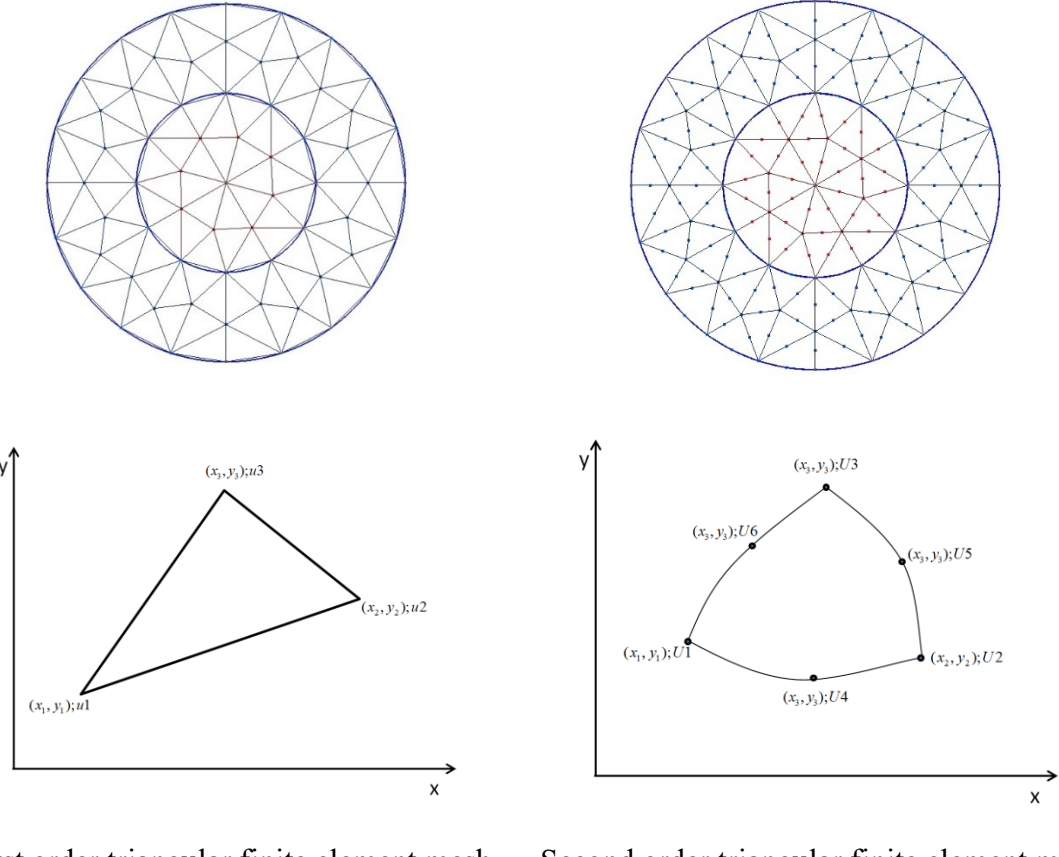
$$\mathbf{D} = \epsilon \mathbf{E} \quad (2.23)$$

$$\mathbf{J} = \sigma \mathbf{E} \quad (2.24)$$

In the above expression  $\mu$  is the magnetic permeability,  $\epsilon$  is the electrical permittivity and  $\sigma$  is the electric conductivity of the material. For an isotropic material these quantities are scalar values, but when the material is of an anisotropic nature, a tensor form of the above constants is needed.

### 2.3 FINITE ELEMENT METHOD

The finite element analysis of a problem starts with the division of the geometric model into small domains i.e. the mesh generation process. The discretized form, which contains a certain number of small elements of predefined shape, are later formulated with numerical analysis (differential equations). The approximate solution for the implied equations is derived for each element by a polynomial entity. Figure 2.3 shows the basic two dimensional (2D) meshes for two concentric circular surfaces considering first order and second order elements cases. For developing basic understanding out of various categories for mesh elements, only triangular element type is shown here.



First order triangular finite element mesh      Second order triangular finite element mesh

*Figure 2.3 Mesh with basic triangular element*

As seen from the structure of a single element for both first order and second order mesh, each node of an element carries some potential ‘U’ which defines the field. The primary motive in FEM is to solve this potential, which will then be used in obtaining different field quantities. The finite element solution starts by deriving the shape functions  $N_i$  in an element.

There are two approaches in defining shape functions: i) nodal element ii) edge element

Based on those shape functions we compute the potential over nodes or edges:

$$U(x_i, y_i) = \sum_{i=1}^m N_i(x, y) U_i \quad (2.25)$$

In our case the potential  $U$  is the magnetic vector potential  $\mathbf{A}$ . The same nomenclature is used in succeeding part of literature.

### 2.3.1 Nodal Element

The shape functions can be obtained by two methods: Lagrange Interpolation and Polynomial Basis. The method of Lagrange Interpolation is widely used for deriving higher order shape functions for both two dimensional and three dimensional element mesh models. (Luomi, 1993).

The generalized form of Lagrange polynomial can be given by

$$L_r(c) = \prod_{\substack{j=0 \\ j \neq i}}^r \frac{(c - x_j)}{(x_i - x_j)} \quad (2.26)$$

where,  $r$  is the degree of polynomial to be interpolated and  $c$  is the variable for space between nodes. The preceding node is specified as ‘ $i$ ’ and ‘ $j$ ’ is succeeding node, so when the solution is at the last node,  $j$  will have value zero. The derived Lagrange polynomial is multiplied with  $m^{th}$  order shape and the area coordinate  $\Lambda$  for obtaining the shape function for the element.

$$N_{ijk} = L_i^i(m\Lambda_1) L_j^j(m\Lambda_2) L_k^k(m\Lambda_3) \quad (2.27)$$

In FEM, the convenient approach to obtain shape function is by establishing the element parameters in the reference coordinate system. Formation of shape function in reference element is an easy task. In the later part simple coordinate transformation is needed for obtaining the corresponding shape function on global coordinates.

### 2.3.2 Edge Element

In the previous method the shape functions were derived for each node, which is a widely used approach. However, the nodal approach leads to some abnormalities while deriving the magnetic field solutions at sharp edges (the detailed explanation is laid in subsequent section). This issue can be handled by the use of the edge element approach. Here, the shape functions are derived for the edges and the magnetic vector potential is given by

$$\mathbf{A} = \sum_{i=1}^{n_e} \alpha_i \mathbf{N}_i \quad (2.28)$$

Where,  $\alpha_i$  is the line integral of the tangential component of the vector potential at edge  $i$ ,

$$\alpha_i = \int_i \mathbf{A} \cdot \boldsymbol{\tau} dl \quad (2.29)$$

here  $\boldsymbol{\tau}$  is unit tangent vector. In the expression (2.28)  $\mathbf{N}_i$  is the edge basis function at edges ( $i=1, 2, \dots, n_e$ ) of the finite element mesh (Webb, 1993).

$$N_i = \ell \eta - N_n^1 \nabla N_m^1 \quad (2.30)$$

$N_m^1$  is the first order shape function at nodes 1, 2, 3, 4, 5 and 6.  $\ell$  is the length of edge  $i$  connecting nodes  $m$  and  $n$ . Figure 2.4 shows the realization of the edge element shape function for first order 3D tetrahedral element.

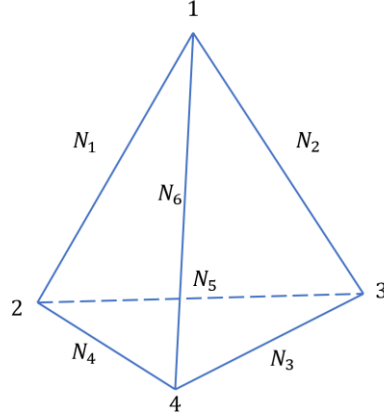


Figure 2.4 Edge basis First order tetrahedral element

Edge basis shape function in the above case are given by equation 2.30

$$\begin{aligned} N_1 &= L_1 \left( N_1^1 \nabla N_2^1 - N_2^1 \nabla N_1^1 \right) \\ N_2 &= L_2 \left( N_1^1 \nabla N_3^1 - N_3^1 \nabla N_1^1 \right) \\ N_3 &= L_3 \left( N_3^1 \nabla N_4^1 - N_4^1 \nabla N_3^1 \right) \\ N_4 &= L_4 \left( N_4^1 \nabla N_2^1 - N_2^1 \nabla N_4^1 \right) \\ N_5 &= L_5 \left( N_2^1 \nabla N_3^1 - N_3^1 \nabla N_2^1 \right) \\ N_6 &= L_6 \left( N_4^1 \nabla N_1^1 - N_1^1 \nabla N_4^1 \right) \end{aligned}$$

The edge basis potentials obtained from (2.28), are used in Galerkin's weighted residual method below for further evaluation of exact solution. The method involves application of shape functions as weight functions  $\eta$  (Råback *et. al.*, 2016).

$$\begin{aligned} &\int_{\Omega} \left\{ \sigma \frac{\partial \mathbf{A}}{\partial t} \cdot \boldsymbol{\eta} + \sigma \nabla V \cdot \boldsymbol{\eta} + v (\nabla \times \mathbf{A}) \cdot (\nabla \times \boldsymbol{\eta}) \right\} d\Omega \\ &- \int_{\partial\Omega} \{ (v (\nabla \times \mathbf{A}) \times \boldsymbol{\eta}) \cdot (\mathbf{n} \times \boldsymbol{\eta} \times \mathbf{n}) \} dS = \int_{\Omega} \{ \mathbf{J}_s \cdot \boldsymbol{\eta} \} d\Omega \end{aligned} \quad (2.31)$$

In the above expression  $v=1/\mu$  i.e the reluctivity term and  $V$  is the reduced scalar potential for the electric field  $\mathbf{E}$ . The magnetization of material in AMB has a non-linear behavior. This non-linearity is modeled with a single valued cubic monotonic spline B-H curve of material (Ref. Appendix I). For solving the nonlinear system, Newton-Raphson iterative method is applied.

The present work of thesis concentrates on the application of the edge element approach for second order 3D tetrahedral elements. To maintain the focus of work the mathematical formulations behind higher order edge elements are kept aside from the thesis literature. However, the thorough understanding can be developed from the work of Bergot *et. al.* (2011)

## 2.4 EDDY CURRENT FORMULATIONS

It can be seen from figure 2.2 that the eddy currents are induced due to the time varying magnetic field produced from the source currents. The dependence of the field in the iron on the coil current arises the need of solving both the electric and magnetic fields together. As per figure 2.2, the eddy current problem is consisting of eddy current region with specific conductivity and it is surrounded by non-conducting media (in our case it is air). The current source causing the field is located at the vicinity of air. The interface between air and conducting region bounds the eddy currents. The magnetic field has been defined in both conducting and non-conducting region. The electromagnetic field in conductors can be derived using two basic formulations viz. i)  $\mathbf{A}$ - $V$  Formulation and ii)  $\mathbf{T}$ - $\varphi$  Formulation.

The former is to use a magnetic vector potential  $\mathbf{A}$  and an electric scalar potential  $V$  hence referred as  $\mathbf{A}$ - $V$  formulation.

In equation 2.14, the flux density can be shown in the form of rotational derivative of the vector potential as

$$\mathbf{B} = \nabla \times \mathbf{A} \quad (2.32)$$

From 2.14 and 2.30, the electric field producing the magnetic field is expressed in terms of magnetic vector potential  $\mathbf{A}$  and reduced scalar potential  $V$  of the field.

$$\nabla \times \mathbf{E} = -\nabla \times \frac{\partial \mathbf{A}}{\partial t} \quad (2.33)$$

$$\mathbf{E} = -\frac{\partial \mathbf{A}}{\partial t} - \nabla V \quad (2.34)$$

The other way of obtaining the electromagnetic field solution is by solving the electric vector potential  $\mathbf{T}$  and the magnetic scalar potential  $\varphi$ . The formation is well known as  $\mathbf{T} - \varphi$  formulation

$$\mathbf{J} = \nabla \times \mathbf{T} \quad (2.35)$$

$$\mathbf{H} = \mathbf{T} - \nabla \varphi \quad (2.36)$$

Since, in the present task is nowhere focused on above  $\mathbf{T} - \varphi$  formulation; the pertaining discussion carried out is for the formulation with  $\mathbf{A}$  and  $V$ . The work involves the use of  $AV\text{-}\mathbf{A}$  formulation explained in subsequent section. However, thorough treatment of various formulations used for eddy current problems can be found in (Biro, 1999). The work of Renhart et.al (1988) portrays good comparative study of  $AV\text{-}\mathbf{A}$  and  $\mathbf{T} - \varphi$  formulations.

#### 2.4.1 AV-A Formulation

The difficulties arise while interfacing different sets of potentials at the conductor surfaces, which are used in both conductors and eddy current-free regions (Biro, 1990). This problem can be avoided if the potentials  $\mathbf{A}$  and  $V$  in conductors are coupled with  $\mathbf{A}$  outside the conductors. From (2.9), (2.19), (2.32) and (2.34), driving equations in AVA formulation are expressed below (Råback *et. al.*, 2016):

In eddy current region let's say  $\Omega_1$

$$\nabla \times \left( \frac{1}{\mu} \nabla \times \mathbf{A} \right) = -\sigma \frac{\partial \mathbf{A}}{\partial t} - \sigma \nabla V + \mathbf{J}_s \quad (2.37)$$

$\mathbf{J}_s$  is the impressed current density or source term for the above mathematical expression and its divergence free nature (Biro, 1990) can be formulated as

$$\nabla \cdot \left( \sigma \frac{\partial \mathbf{A}}{\partial t} + \sigma \nabla V \right) = 0 \quad (2.38)$$

In eddy currents free region ( $\Omega_2$ ) solely source current is flowing. The current density,  $\mathbf{J}_s$  in the region  $\Omega_2$ , is covered with  $\partial\Omega$  boundary and its expression can be laid as

$$\nabla \times \left( \frac{1}{\mu} \nabla \times \mathbf{A} \right) = \mathbf{J}_s \quad (2.39)$$

Alternatively, the above form can be reformulated as

$$\nabla \times \mathbf{H} = \mathbf{J}_s \quad (2.40)$$

For obtaining eddy current in the entire region, the method of Galerkin's weighted residual (2.31) is applied. During the solution process, the boundary condition  $\mathbf{A} \times \mathbf{n} = 0$  is set at the boundaries.

In the problem region, the continuity of  $B \cdot \mathbf{n}$  is ensured by the continuity of  $\mathbf{A}$ . The required continuity of  $\mathbf{H} \times \mathbf{n}$  is satisfied naturally during the process of Galerkin formulation (Biro, 1990).

The  $AV\text{-}\mathbf{A}$  approach involves a large number of unknowns in the eddy current-free region and these makes the solution time consuming. The source requires accurate modeling to fetch fairly close results otherwise the error margin can be high. However, with such coupled formulation, multiple connected domains are possible to solve without any other extra considerations (Renhart *et. al.*, 1988). This is the big advantage which supersedes the above limitations.

The eddy current formulation discussed in the preceding section is implemented in the open source software Elmer for electromagnetic modeling. The feature is utilized here for the evaluation of eddy currents.

## 2.4.2 Eddy Current Solutions with application of Edge Element through Elmer

In the study made by Biro (1999), out of all the formulations, the most efficient way is to take the Coulomb gauge on the vector potentials in the driving equations. The technique shows promising and robust numerical realization with nodal finite element. The difficulty with the nodal approach is faced when two different type of problem definitions are involved in the model. The example of the same can be realized in Figure 2.2, where non-magnetic and non-conducting entity (air) is surrounding highly permeable and conducting body (iron). The use of nodal FEM in such problem involves the use of the magnetic vector potential  $\mathbf{A}$  in iron and the electric scalar potential  $V$  is defined in air. The resulting evaluation will lead to a weak coupling between both potentials and make the approach unsuitable for the defined problem. The vector potential  $\mathbf{A}$  can't be employed in air, as the normal component  $\mathbf{A} \cdot \mathbf{n}$  is continuous and at same time it has to be defined as discontinuous at all interfaces. Considering the above facts, the evolved errors are no more trivial. The problem is also faces at the sharp corners. The rotational derivative of  $\mathbf{A}$  is considered continuous when tangential component of the vector potential is maintained continuous. For the sharp edges this is not accurately seen, hence the field on both side of the corner will be considered independent (Biro, 1999). However, the above factors drastically complicate the solution.

The issues can be circumvented by the use of *Edge Finite Element Method* (Preis *et. al.*, 1991). As seen before, in this method of FEM the vector potentials are approximated over the edges of the element. The approach provides relaxation on required condition of normal component vectors and limits the need for continuity of the tangential vectors over edges. The mechanism of obtaining the field solution in eddy current conducting region using edge element is enumerated in 2.3.2 section.

Edge elements were initially described as Whitney elements, after the name of the mathematician Hassler Whitney who introduced them for the first time in 1957 (Reddy *et. al.*, 1994). But their application in Electromagnetics was realized in late 1980s by Bossavit (1989). The advantage cited for sharp edges before, is the main reason, which makes the edge element approach more viable, as singularities at sharp edges can be dealt without considering any special functions (Webb, 1993).

In Elmer, the “WhitneyAVSolver” is designed with Edge basis formulation to evaluate the magnetic vector potential variable  $\mathbf{A}$ . The scalar potential  $V$  is approximated with the classical Lagrange interpolation. For computing the derived field, “MagnetoDynamicsCalcFields” solver is utilized. This solver applies nodal elements approach for the approximation of the field quantities (Råback *et. al.*, 2016).

## 2.5 MAGNETIC FORCE EVALUATION

The main task of AMB is to produce the required force for levitating the rotor. As discussed before, many aspects affect the maximum force capacity of the actuator. The magnitude of force over all air gaps requires an accurate evaluation. In section 2.1.1 we saw the approach with the fundamental steady state formulae for evaluating the static force. The method can be extended to other numerical methods, where the stiffness terms can be obtained based on the finite difference of the available forces. However, inaccuracy will be magnified when there are measurement errors (Coulomb, 1983). To achieve reasonable results FEM is the most viable approach over all analytical and numerical methods. The magnetic force calculation in present work is carried out with the generalized nodal forces approach in FEM.

The Maxwell stress tensor and the virtual work methods are the two widely used methods for magnetic force computation in finite element analysis. The former is based on a stationary property of the field solution. The electromagnetic force is obtained as a surface integral of the stress tensor. However, in that method there should be a careful selection of the integration surface, otherwise it can drastically affect the accuracy of the results. The method also faces difficulties in problems with sharp edges and small gaps. The second approach for force computation is basically the Coulomb’s method by virtual work principle (Coulomb, 1983). In this method the magnetic energy of one element is

differentiated with respect to a virtual displacement of the nodes of that element (Belahcen, 2004). Since this thesis work is focused on the application of nodal force approach, Maxwell stress tensor will not be carried further in discussion. However, the application of Maxwell stress tensor in modeling linear actuator using FEM is described by Sadowski (1996). The same fundamental can also be applied for modeling axial active magnetic bearing.

### 2.5.1 Nodal Force method:

The principle of virtual work or Local Jacobian derivative for computing total force has been described by Coulomb (1983). The algorithm can be easily implementing in finite element tool without complexities (Coulomb, 1983). A. Bossavit introduced a method to compute the local force in magnetized bodies (Bossavit, 1992). The method is based on the differentiation of the magnetic co-energy or energy under edge element feature.

The use of Maxwell's stress tensor with nodal force method is presented by Kameari (1993). This method is also based on partial derivative of energy or co-energy within the element with respect to the virtual displacement of the nodes in that element.

$$W = \int_V \left( \int_0^B \mathbf{H} \cdot d\mathbf{B} \right) dV \quad (2.41)$$

Where  $W$  is the energy functional of the system represented by the magnetic field strength  $\mathbf{H}$  and the magnetic flux density  $\mathbf{B}$  vectors. The change in energy with displacement is termed as a force and it is given by

$$\mathbf{F} = - \frac{\partial W}{\partial \mathbf{p}} \quad (2.42)$$

where  $\mathbf{F}$  is force vector and  $\mathbf{p}$  is the vectorial direction of virtual displacement.

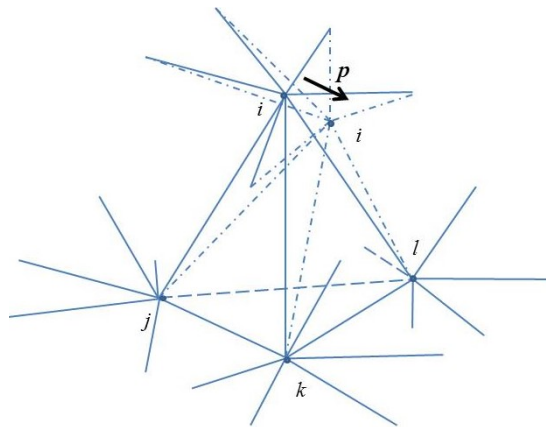


Figure 2.5 Nodal displacement in the Tetrahedral first order element

As showing in figure 2.5, the force will be evaluated for the nodal displacement of the  $i^{th}$  node in  $\mathbf{p}$  direction. Hence the force in each element (e) is expressed as (Belahcen, 2004)

$$F_e = -\frac{\partial}{\partial \mathbf{p}} \int_{V^e} \left( \int_0^B \mathbf{H} \cdot d\mathbf{B} \right) dV^e \quad (2.43)$$

$$\mathbf{F}^e = - \int_{V^e} \left( \frac{\partial}{\partial \mathbf{p}} \left( \int_0^B \mathbf{H} \cdot d\mathbf{B} \right) \left| \mathbf{J}_M \right| + \left( \int_0^B \mathbf{H} \cdot d\mathbf{B} \right) \frac{\partial \left| \mathbf{J}_M \right|}{\partial \mathbf{p}} \right) dV^e \quad (2.44)$$

In the above formulation  $\mathbf{J}_M$  is Jacobian matrix for the transformation from the actual element to the reference one.

The virtual work principle based on the magnetic energy is satisfied by the use of flux conserving transformation (Belahcen, 2004). Under this hypothesis, the magnitude of the flux density stays unchanged during the displacement of elements nodes. For attaining this, the magnetic vector potential is made constant while differentiating the energy. The second approach is using the co-energy, where the derivative of the magnetic co-energy is taken with respect to the virtual displacement at a constant current (Pyrhonen *et. al.*, 2009).

From the material equation (2.22),  $\mathbf{H} = \frac{1}{\mu} \mathbf{B}$ , with substitution in the above equation, the resultant force expression is given by

$$\mathbf{F}^e = - \int_{V^e} \left( \frac{1}{2} \frac{1}{\mu} \frac{\partial \mathbf{B}^2}{\partial \mathbf{p}} \left| \mathbf{J}_M \right| + \frac{\partial \left| \mathbf{J}_M \right|}{\partial \mathbf{p}} \frac{1}{2} \frac{\mathbf{B}^2}{\mu} \right) dV^e \quad (2.45)$$

In the Elmer software flux conserving is achieved with the Piola Transformation. The principle is implemented by substituting the flux density magnitude in the product with the displacement factor  $f_s^{-1}$  in equation (2.43) (Kataja *et. al.*, 2015).

$$\mathbf{B}_s = \frac{1}{\det \mathbf{J}_M} \mathbf{J}_M \mathbf{B} \cdot f_s^{-1} \quad (2.46)$$

where, ‘s’ is displacement parameter. The expression is established from work of Kameari (1993). The derived equations are given by :

$$\mathbf{F}^e = - \int_{V^e} \left[ \left( \mathbf{H} \cdot \mathbf{B} \cdot \frac{\partial \mathbf{J}_M}{\partial \mathbf{p}} \right) - \left( \frac{\partial \left| \mathbf{J}_M \right|}{\partial \mathbf{p}} \cdot \mathbf{H} \cdot \mathbf{B} \right) + \left( \int_0^B \mathbf{H} \cdot d\mathbf{B} \right) \frac{\partial \left| \mathbf{J}_M \right|}{\partial \mathbf{p}} \right] dV^e \quad (2.47)$$

$$\mathbf{F}^e = - \int_{V^e} \left[ \left( \frac{\mathbf{B}^2}{\mu} \cdot \frac{\partial \mathbf{J}_M}{\partial \mathbf{p}} \right) - \left( \frac{\partial |\mathbf{J}_M|}{\partial \mathbf{p}} \cdot \frac{\mathbf{B}^2}{\mu} \right) + \frac{1}{\mu} \left( \frac{\mathbf{B}^2}{2} \right) \frac{\partial |\mathbf{J}_M|}{\partial \mathbf{p}} \right] dV^e \quad (2.48)$$

$$\mathbf{F}^e = - \int_{V^e} \left[ \left( \frac{\mathbf{B}^2}{\mu} \cdot \frac{\partial \mathbf{J}_M}{\partial \mathbf{p}} \right) - \frac{1}{2} \left( \frac{\mathbf{B}^2}{\mu} \cdot \frac{\partial |\mathbf{J}_M|}{\partial \mathbf{p}} \right) \right] dV^e \quad (2.49)$$

The Jacobian matrix is obtained as the derivatives of the shape functions in the reference coordinates,  $\xi$ ,  $\eta$  and  $\Upsilon$ , with respect to the local coordinates  $x$ ,  $y$  and  $z$ .

$$\mathbf{J}_M = \begin{bmatrix} \sum_{i=1,n} \frac{\partial N_i}{\partial \xi} x_i & \sum_{j=1,n} \frac{\partial N_j}{\partial \xi} y_j & \sum_{j=1,n} \frac{\partial N_j}{\partial \xi} z_j \\ \sum_{i=1,n} \frac{\partial N_i}{\partial \eta} x_i & \sum_{i=1,n} \frac{\partial N_i}{\partial \eta} y_i & \sum_{j=1,n} \frac{\partial N_j}{\partial \eta} z_j \\ \sum_{j=1,n} \frac{\partial N_j}{\partial \Upsilon} x_j & \sum_{j=1,n} \frac{\partial N_j}{\partial \Upsilon} y_j & \sum_{j=1,n} \frac{\partial N_j}{\partial \Upsilon} z_j \end{bmatrix} = \begin{bmatrix} J_{11} & J_{12} & J_{13} \\ J_{21} & J_{22} & J_{23} \\ J_{31} & J_{32} & J_{33} \end{bmatrix} \quad (2.50)$$

And the determinant of  $\mathbf{J}$  is given by

$$|\mathbf{J}_M| = J_{11}(J_{22}J_{33} - J_{32}J_{23}) - J_{12}(J_{21}J_{33} - J_{31}J_{23}) + J_{13}(J_{21}J_{32} - J_{22}J_{31}) \quad (2.51)$$

In the above method, the force being an integration over an element, the field quantities don't require any spatial differentiation. This relaxes the computation from considering discontinuous field. The total force (global force) on a body can be obtained easily just by summation of the nodal forces (kameari, 1993).

The nodal force computation provides accurate results at lower mesh density compare to Maxwell stress tensor. This is due to the fact that the force is evaluated from the energy instead of the derived field quantities from magnetic vector potential. (Belahcen, 2004).

## 2.6 METHODOLOGY

The intention was to produce a dynamic solution for the axial AMB under biased sinusoidal excitation. The simulation is current driven with 50hz frequency. For avoiding the effect of high transients, the simulation is started from solutions obtained with static simulation. The static simulation is carried out with DC current of 5A bias level. The static solution is also referred as initial field solution in the present work. The time stepped simulation for sinusoidal excitation is then start from the available initial field solution. In both of the simulations, the shaft is considered to be in steady position.

For making above simulations current driven, the current density vectors in the coil, are defined under the physical coordinate system. The model is bounded in a cylinder and on the outer most surface of the cylinder, dirichlet conditions are define for tangential component of the vector protection  $\mathcal{A}$ .

# CHAPTER 3

## STATIC MODEL

This chapter provides details about the static simulation carried out during this work. In the beginning of the chapter, constructional details of the physical and 3D finite element model are explained. The definitions and parameters used are explained in subsequent section. At the end, the simulation results for the static case and their role in the study are explained.

### 3.1 OVER VIEW OF MODEL

The axial magnetic bearing used in this work was studied previously by Tommila (2002). The analytical approach used was based on the method articulated by Kucera L. *et. al.*(1996). In the present task, the model dimensions including material data are considered from the work of Tommila (2002). However, the comparative analysis was limited to 2D and 3D FEM, hence comparison with analytical approach is not stressed here. The model is also referred as AXB55 in subsequent discussions.

In the current-controlled actuator, the operation with biased current is a traditional way to linearize the nonlinear current-force relationship. This linearizes the dependence of the bearing force on the control current. In AXB55 model,  $I_{max}$  is 7.5A while  $I_{bias}$  is 5A and these considerations are just for study purpose. For computing the force and the flux density curves, simulations are carried out at different bias levels. These will help in understanding the behavior of the magnetic circuit under different current magnitudes. Another practical purpose of this simulation was to attain a field solution at steady state point. The field solution obtained over here will then become the starting point for the time stepped simulation for further analysis.

#### 3.1.1 Construction

As shown in figure 3.1, the magnetic circuit for the actuator consists of 5 sections, viz. coil, yoke, disc, shaft (rotor), and air. The geometry is developed in GMSH open source tool and the sectional view of the model including its dimensions is provided in Appendix II. The model is axis symmetric over z-axis.

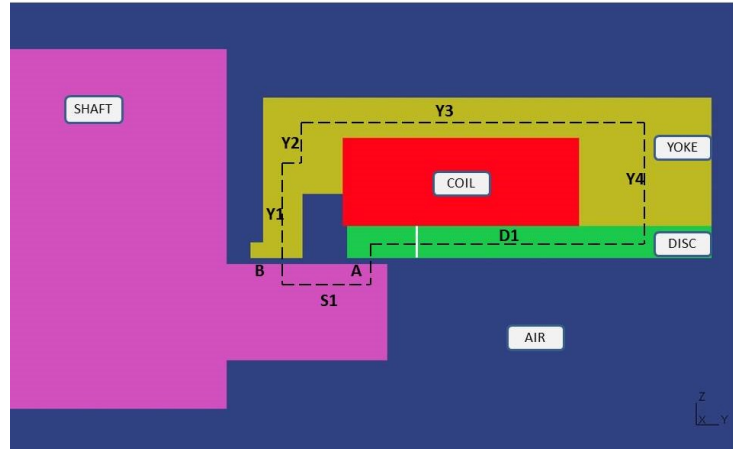


*Figure 3.1 Cross Sectional View of AXB55 Actuator*

In the model, the yoke and the disc are constructed from Imatra520 Steel, while the shaft is manufactured from Imacro steel. The magnetizing properties used for both materials are specified in Appendix I. The magnetic properties are defined using nonlinear single valued H-B curves. The actuator coil is formed from copper conductor and it consists of 150 turns.

### 3.1.2 Mesh

The mesh in 3D model is created to match the 2 dimensional mesh model. The second order tetrahedral elements are used for the field calculation in the actuator. A relatively dense mesh is considered in the disc and yoke for better calculation of eddy current losses. The shaft surface close to the air, also consist of denser mesh to achieve precise force computation. The 2-D reference mesh and 3D mesh used are shown in the figure 3.2 and figure 3.3 respectively.

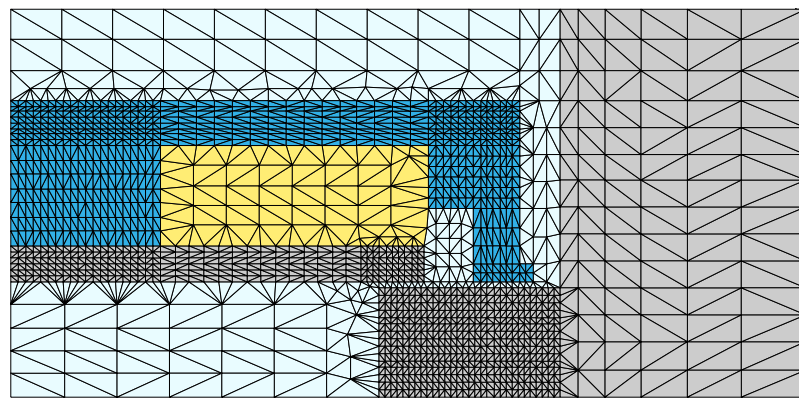


*Figure 3.2 Reference 2D Model Mesh*

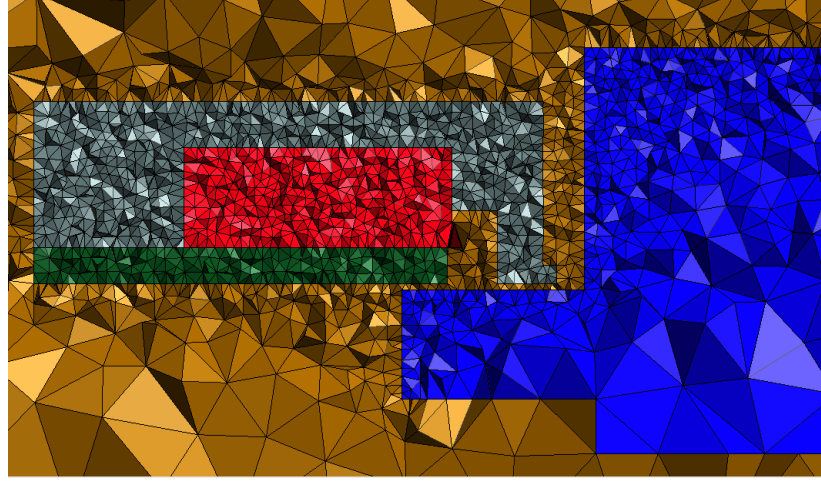


*Figure 3.3 3D model Mesh with tetrahedral element*

There is consideration of skin depth factor in deciding the height of element. The yoke and disc have dense mesh divisions so that skin effect in those regions can be captured accurately. The skin effect study is necessary to evaluate the effects from eddy currents that flow through iron part. Hence, the skin depth function can be used to generate a structured mesh (as shown in Figure 3.2). The height of the elements in the orthogonal direction of the flux can be decided based on the penetration depth  $h$  in (2.8). The expression can also be given by:

$$h = \sqrt{\frac{2}{\sigma\mu\omega}} \quad (3.1)$$

where,  $\omega$  is angular frequency and  $\sigma$  is the conductivity.

As per the theory laid by Meunier (2010), this consideration helps in achieving two things: i) Accurate evaluation of the offsets in the magnetic flux distribution caused by the skin effect and ii) The mesh generated will be capable of evaluating the effects of eddy currents. However, the mesh in 3D was generated in GMSH open source tool, which would require intense coding for controlling the element height in a particular direction. This reason led to the use of a simple unstructured tetrahedral mesh. The mesh element size factors were controlled for the yoke and the disc area to achieve a compatible mesh density. As such, the required height is 1.216 mm based on 50Hz frequency, approximate permeability  $\mu=0.001$  Tm/A and  $4.3 \times 10^6$  A/m<sup>2</sup> of conductivity in the disc region. With the obtained visual data from 3D mesh, it consists of 5 elements in the orthogonal direction at 50 mm radius in the disc. This makes an element height of about 0.8 mm (approx.) for a 4 mm thick section of the disc, which is less than 1.216 mm. This already sufficed the required mesh density. It must be noted that the optimal element height can prevent the oversizing of problem.

## 3.2 MODEL PARAMETERS

### 3.2.1 Boundary Condition

The model consists of 3D closed coil, hence current driven simulation is used in the present work. The current produces the required field oriented in the flux path as show in Figure 3.1.

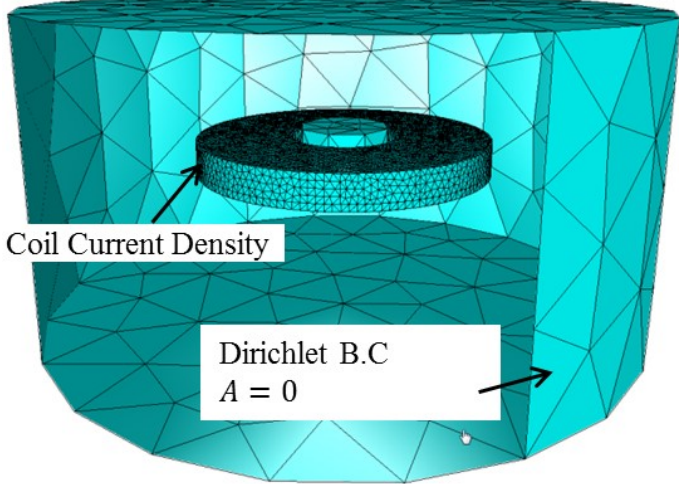


Figure 3.4 3D model with cylindrical boundary

For the uniqueness of the field solutions, the normal components of the flux density  $\mathbf{B}$  and the current density  $\mathbf{J}$  must vanish at the interfaces for simply connected domains. However, the solutions of the defined problem are obtained with quasistatic approximation. This fulfills both criteria in a natural manner (Biro O. et. al., 2005). For limiting the problem domain, the actuator is surrounded by a closed cylinder which forms an air region cylinder as shown in Figure 3.4. The normal component of the flux density must be zero on the outer surface of this cylinder. In Elmer, this condition can be achieved by setting the tangential component of  $\mathbf{A}$  to zero and the fact is supported by equation (2.32).

Since the simulation is current driven, the current density term is used as body force in the coil. This is achieved by defining the vector equations of the current density in the physical coordinate system. The coil is oriented in x-y axis hence following the definitions of the current density, the input serves the purpose.

$$J_x = |J| * \frac{\hat{y}}{\sqrt{\hat{x}^2 + \hat{y}^2}} \quad (3.2)$$

$$J_y = |J| * \frac{x}{\sqrt{\hat{x}^2 + \hat{y}^2}} \quad (3.3)$$

$$J_z = 0 \quad (3.4)$$

### 3.2.2 Parameters

For the steady state solution the model is simulated with DC bias current of 5A. In Elmer this is defined by a current density magnitude  $|J|$  which is obtained from the current and the cross section area for coil.

No. of Turns in coil:	150 T
No. of coil :	1
DC Current per coil/per turn:	5 A
Total current from cross-section for model:	375 A-T
Coil height:	11 mm
Coil width:	29.5 mm
Total cross sectional area:	324.5 mm <sup>2</sup> 0.0003245 m <sup>2</sup>
Current density for model:	2.3112E+06 A/m <sup>2</sup>

The material list including relevant properties used in the simulation is mentioned in table 3.1 below.

Table 3.1 Material list

Body Index	Body name	Material	Electrical conductivity [1/Ωm]	Relative Permeability ( $\mu_r$ )
1	Yoke	Imatra 520	4.30E+06	from material curve
2	Disc	Imatra 520	4.30E+06	from material curve
3	Coil	Copper	0	1
4	Rotor	Imacro	4.30E+06	from material curve
5	Air	Air	0	1

There were certain assumptions and considerations made before the simulation:

- i) Switching harmonics from the supply amplifier are neglected while modeling the current density equations.
- ii) The insulation is considered to be negligible while preparing the model.
- iii) The mesh density in air, conductor and shaft are arbitrarily chosen without any prior considerations.
- iv) The shaft is considered to be at steady state position.
- v) Eddy Current losses in the coil conductor are neglected from the analysis.

### 3.3 Results and Observations

The simulations of the three dimensional model of the AXB55 are carried out in ELMER software. It includes various physical models for solving the problems from various fields. In solving the model of the thesis, MagnetoDynamics solver has been utilized. The model solves the required potentials in the mesh and which is then followed by MagnetoDynamicsCalcFields solver for the evaluation of the field solutions.

The present section portrays the results which are post processed by using MATLAB and PARAVIEW software. The results in matrix form are processed with MATLAB whereas visualization of the output files in .vtu format is done with PARAVIEW. Elmer provides a facility in deciding the file formats for post processing.

#### 3.3.1 Flux Density Distribution:

The flux density distribution in 2D and 3D models can be seen from the Figure 3.4 and Figure 3.5 respectively. The distribution in both cases is visually identical. Some part of the yoke and disc observe very high flux density. The flux density plots in both cases are captured at 5A DC current input to coil.

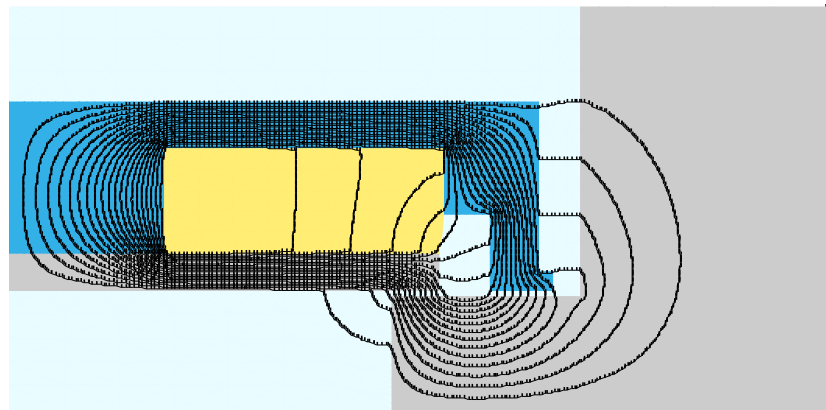
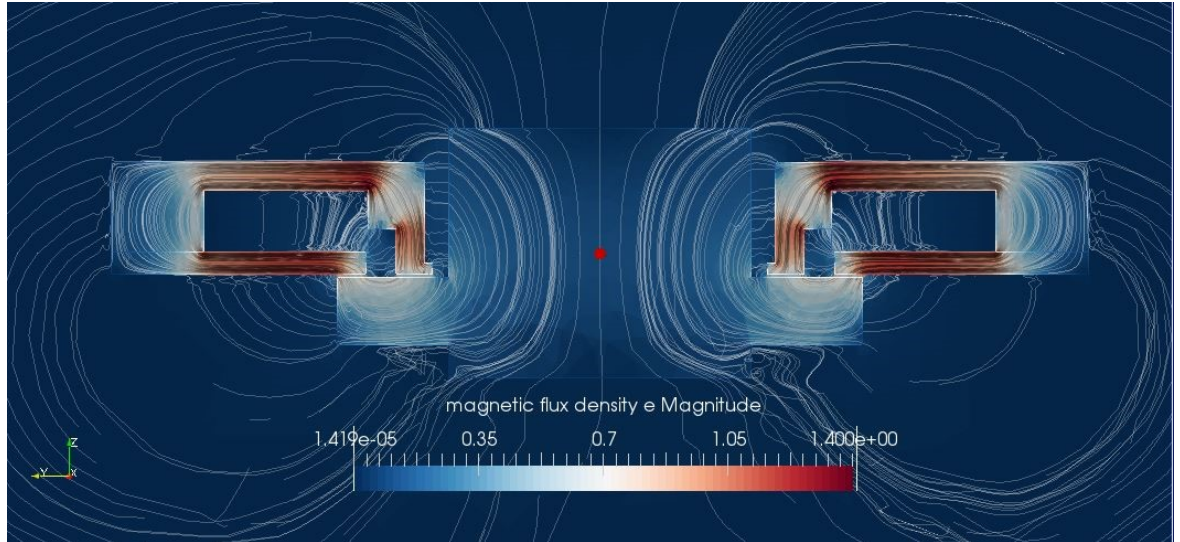


Figure 3.4 Flux Density Distribution in Two Dimensional Model



*Figure 3.5 Flux Density Distribution in Three Dimensional Model*

The saturation limits in iron parts (in both yoke and disc) decide the maximum flux producing capacity and hence the loading limits of actuator. For the evaluation of the force distribution, the study of the flux densities in the air gaps will be more interesting. Here, we can also see how the saturation in iron is affecting the force for the defined air gap length. The comparative data of flux density in both air gaps of 3D model are evaluated at the midpoints of the air gaps and are mentioned in Table 3.2.

The results are plotted as function of the coil current magnitude in figure 3.6. In the same plot, the flux density data for the air gaps from the reference model are also marked for further comparison.

Table 3.2 Flux Densities in Air

Current inputs	Ba-Flux Density in Air Gap 'a' (T)		Bb-Flux Density in Air Gap 'b' (T)		Difference in Ba (%)	Difference in Bb (%)
	3D FEM	2D FEM	3D FEM	2D FEM		
0	0.0000	0.0000	0.0000	0.0000	0.0000	0.0000
1	0.1267	0.1291	0.1170	0.1139	1.8490	-2.6880
2	0.2531	0.2580	0.2339	0.2277	1.8851	-2.7120
3	0.3791	0.3865	0.3503	0.3411	1.9264	-2.6844
4	0.5037	0.5137	0.4655	0.4534	1.9452	-2.6505
5	0.6217	0.6343	0.5747	0.5602	1.9936	-2.5784
6	0.7144	0.7311	0.6629	0.6474	2.2787	-2.3860
7	0.7733	0.7921	0.7227	0.7053	2.3751	-2.4670
8	0.8084	0.8291	0.7622	0.7432	2.4999	-2.5654
9	0.8307	0.8536	0.7901	0.7705	2.6847	-2.5499
10	0.8465	0.8714	0.8127	0.7917	2.8545	-2.6526
11	0.8583	0.8850	0.8310	0.8092	3.0186	-2.6948
12	0.8675	0.8960	0.8465	0.8240	3.1760	-2.7315
13	0.8749	0.9050	0.8601	0.8370	3.3326	-2.7674
14	0.8814	0.9127	0.8722	0.8484	3.4274	-2.8003
15	0.8862	0.9193	0.8832	0.8588	3.5968	-2.8417

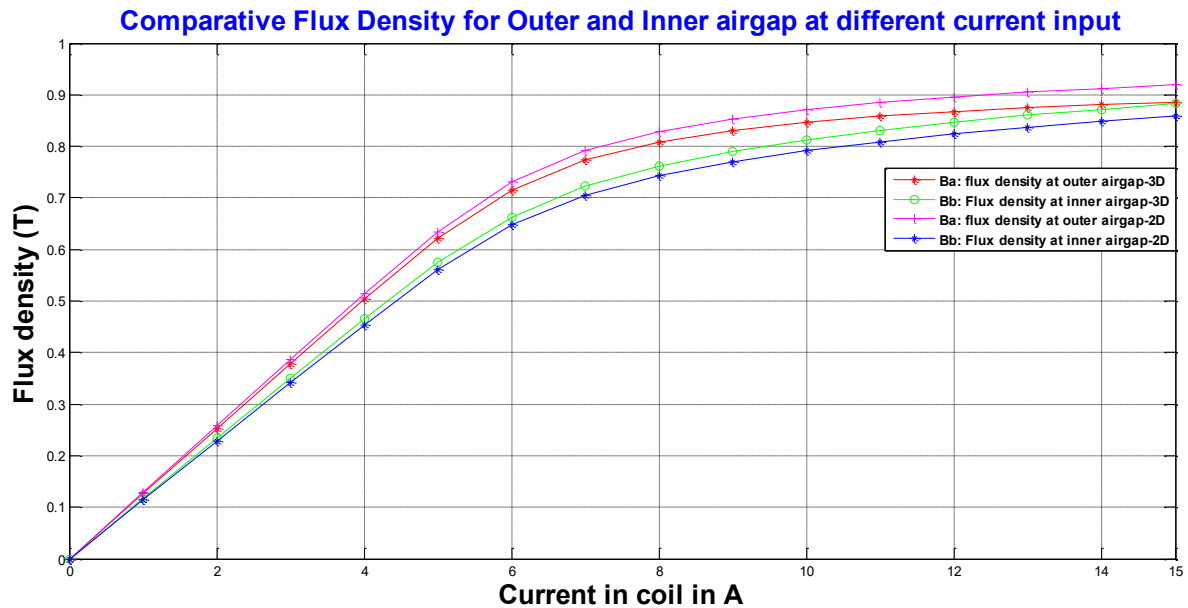


Figure 3.6 Air gap Flux densities at different coil current magnitudes in 3D and 2D FEM

In both cases, the flux density in the inner air gap stays low compared to the outer gap flux density. Prior to the simulation the author speculated that the inner gap flux density

should be higher compared to outer flux density. This assumption was made on the basis of the cross sectional area of the open faces of the yoke and the disc. The cross section area of the open face of the yoke in air gap ‘b’ is  $6.221\text{E-}03 \text{ m}^2$  while for the part of the disc near air gap ‘a’ it is  $3.473\text{E-}03 \text{ m}^2$ . Hence the flux density in the inner air gap has to be higher. However, in reality it is exactly the opposite as the leakage factor was neglected and it drastically affects the flux density distribution. The percentage difference in the flux densities obtained by 3D FEM and the reference 2D FEM computations are plotted in figure 3.7 below.

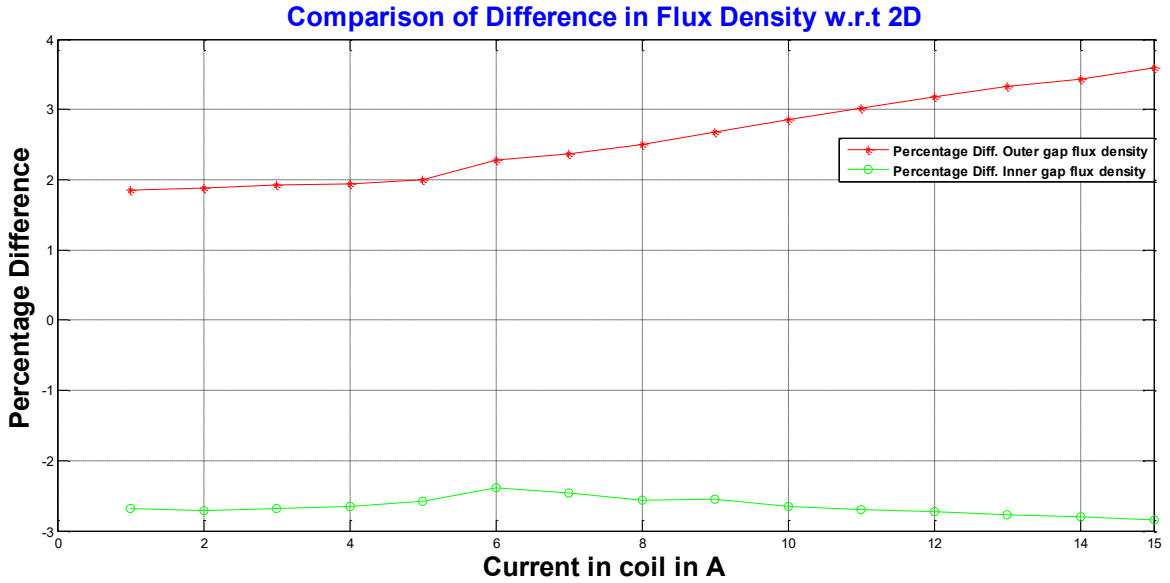


Figure 3.7 Percentage difference in the flux density for 3D FEM with reference to 2D FEM

The difference is considered with respect to 2D FEM results. For three dimensional model, the variations in the flux densities for both air gaps are different compared to the reference plots. The reason behind such discrepancy is difficult to define. However one of the factors is the mesh quality and type. The 3D case is using unstructured mesh with tetrahedral elements while in case of 2D it is structured mesh. The differences in the computed leakage flux in both cases can also affect the results.

### 3.3.2 Magnetic Force Computation:

The Elmer environment provides two options for force computation, namely the Maxwell Stress Tensor and the Generalized nodal force approach (GNF). The GNF approach has been used in present case for the computation of magnetic forces. The total force comes out as a surface integral over shaft body, which is done by Elmer in the background. Table 3.3 shows the values of steady state force computed at different coil current magnitudes. The results extracted from the reference 2D FEM solution are also listed in

the same table. Those values are computed with Arkkio's Method in the in-house software of Sulzer Pump (Finland) Oy.

*Table 3.3 Computed steady state Magnetic Force*

Current inputs	Corresponding current density (A/mm)	Total Force (N)		Difference (%)
		3D FEM	2D FEM	
0	0	0	0	0
1	2.3112	17.63	18.07	2.435
2	4.6225	70.44	72.22	2.465
3	6.9337	158.01	162.1	2.523
4	9.2450	278.99	286.4	2.587
5	1.1556	425.04	436.9	2.715
6	1.3867	562.82	581.7	3.246
7	1.6179	663.46	686.1	3.300
8	1.8490	731.09	756.1	3.308
9	2.0801	778.52	806.4	3.457
10	2.3112	815.42	845.2	3.523
11	2.5424	844.96	876.7	3.620
12	2.7735	869.71	903.2	3.708
13	3.0046	890.84	926.1	3.807
14	3.2357	909.31	946.3	3.909
15	3.4669	926.31	964.3	3.940

The static load capacity, as described by Lantto (1999) is the load under which the bearing is able to lift the rotor up to levitation from the retainer bearings. This also defines the maximum static force limit for the magnetic bearing. For the axial actuator this definition is applicable when the axis of the machine is vertical that is oriented along the gravity.

The force of the bearing depends on the flux density in the air gaps. The current in the coil controls the flux density. The magnetizing force and current relationship is highly nonlinear along the axial direction in our case, which increases the complexity of the control. However by supplying biased current in the actuator coils on both sides, the linearization becomes easier. The detailed understanding can be developed from work of Antila (1998) and Maslen *et. al.* (1993).

The above tabulated results and the difference with respect to the reference results are plotted in Figure 3.8 and 3.9. The results from both cases show similar behavior with a gradual increase in the difference with the current input except for the linear region. A

high difference is observed over there and the practical reason behind such behavior is difficult to state.

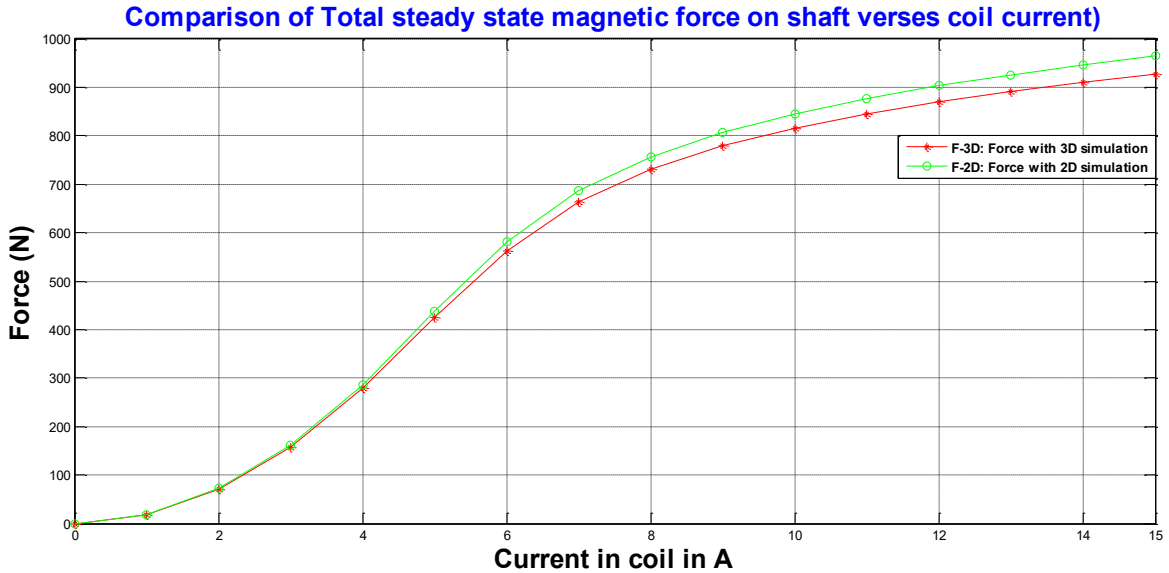


Figure 3.8 Comparative Magnetic force - dc coil current relation in 3D FEM and 2D FEM

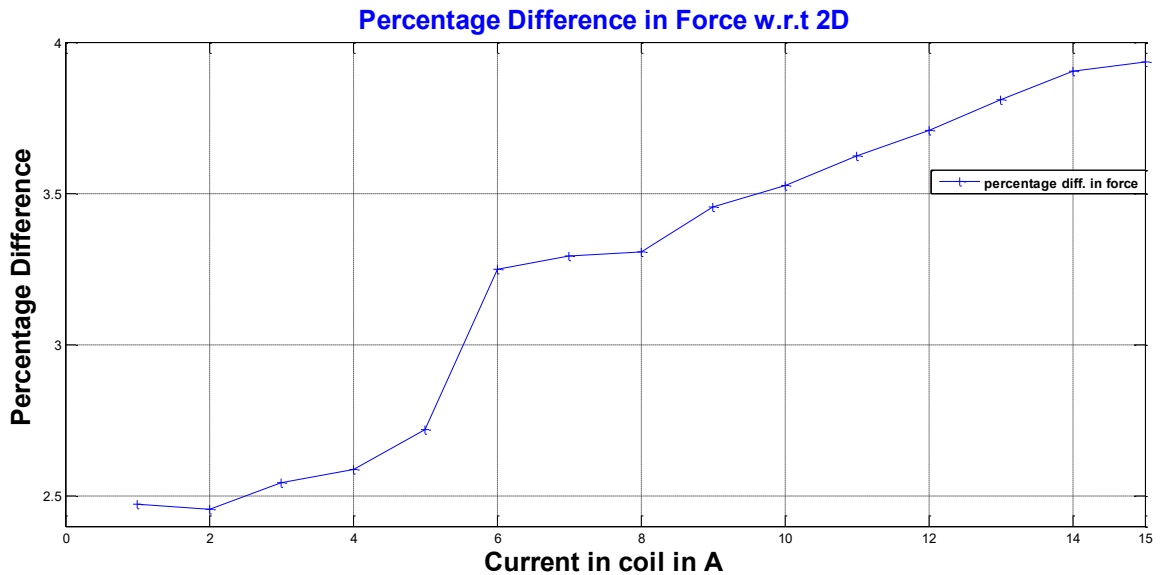


Figure 3.9 Percentage difference in the force results for 3D FEM with respect to 2D FEM

The results in figure 3.8 can be useful to engineers in understanding the linear and nonlinear region of operation. The operation in lower current region can lower the slew rate as change in force against coil current is low. The preferred zone is the linear region. The mentioned characteristics can be linearized using proper combination of control

signal and bias level. The evidence to the mentioned fact can be found in the work of Lantto (1999). It provides detailed information of the force as function of the control current with the verification of results against measurements.

# CHAPTER 4

## DYNAMIC MODEL

The results obtained with time stepped simulations are explained in this section of the thesis. The simulations are carried out in the Elmer software under the category of “transient simulation”. In the axial AMB the control current in the coils should have an adequate magnitude to control the offsets in the axial direction of the rotor. Practically the rotor never stays steady at one position; it follows a pattern of movement and the coil current should be varied accordingly. The varying current will produce a time varying field which leads to eddy currents in the iron parts of the actuator. In the present case, the rotor is practically not moving. However, the high amplitude simulations are carried out by considering a sinusoidal current in the coil. The main focus of this study stays on the eddy current distribution, the evolved magnetic forces and the eddy current power loss.

The 3-D finite element analysis is performed on two types of meshes; firstly for a mesh with first order elements and later with a second order elements mesh. The comparative analysis with respect to two dimensional reference solutions is laid simultaneously. For avoiding initial transients in the signals, the solution is started from the steady solution. The field solution saved at 5A bias level is the starting point for the dynamic case.

### 4.1 MODEL PARAMETERS

The boundary condition in the present case of study stays the same as before. The sinusoidal component is modeled in the previous coil current equation.

$$J_x = \frac{\hat{y}}{\sqrt{\hat{x}^2 + \hat{y}^2}} * (|J| + J_{AC} * \sin \omega t) \quad (4.1)$$

$$J_y = \frac{x}{\sqrt{\hat{x}^2 + \hat{y}^2}} * (|J| + J_{AC} * \sin \omega t) \quad (4.2)$$

$$J_z = 0 \quad (4.3)$$

In the above expression  $J_{AC}$  is the current density for defining the AC component with 2.5A magnitude. The corresponding current density input will be 1.1556E+06 A/m<sup>2</sup>. The same material properties are considered like in the static model. The effect of stress on the B-H loop of material is neglected here for simplification of the problem.

## 4.2 TIME STEPPING:

The results are computed over 3 cycles by the use of 100 time steps per cycle. In Elmer environment the first order time discretization can be done by Backward Difference Formula (BDF) and Crank Nicolson Method. The BDF method can be used up to 5<sup>th</sup> order, but for the simulated model the second order backward difference formula has been used. The accuracy of the method increases with the increase of the order.

The backward difference formulae (Ruokolainen J. et. al., 2016) of first order and second order time derivate are expressed in equation 4.4 and 4.5 respectively

$$\left( \frac{1}{\Delta t} M + S \right) a^{k+1} = F^{k+1} + \frac{1}{\Delta t} M a^k \quad (4.4)$$

$$\left( \frac{1}{\Delta t} M + \frac{2}{3} S \right) a^{k+1} = \frac{2}{3} F^{k+1} + \frac{1}{\Delta t} M \left( \frac{4}{3} a^k - \frac{1}{3} a^{k-1} \right) \quad (4.5)$$

where,  $\Delta t$  is the time step size and  $a^k$  is the solution at  $k^{th}$  time step.  $S$  is associated with the differential operator and  $F$  is a function of spatial coordinates and time. The method to use time stepping technique is explained in chapter 6 of Elmer solver manual by Ruokolainen J. et. al. (2016).

## 4.3 HIGH AMPLITUDE SIMULATIONS

### 4.3.1 Eddy current and Flux Density Distribution

The Elmer 3D FEM environment is designed with the AVA formulation for evaluation of the eddy currents in magneto dynamic problems. The same formulation is used in solving the present model of the thesis. Along with the eddy currents, the flux density distribution is also diligently studied. The evaluation is made for analyzing the variation in the field from the surface of the disc near the coil to the outer surface of the disc. These computations are made at 50 mm radius in the disc. The location is marked with white the line in figure 3.1 and the results are captured over 100 points on that line. For comparative check, the same sets of results are taken from the reference calculation. The reference case is solved with 2D FEM and the mesh consisted of second order elements.

The 3D FEM simulations are carried out for first order mesh and second order mesh. The results of eddy current density distribution in all cases are explained below.

Figure 4.1 demonstrates the variation in eddy current from the disc surface near the coil to the outer surface (exposed to air). The skin effect is accurately captured by the use of second order mesh elements in the reference calculation with 2D mesh.

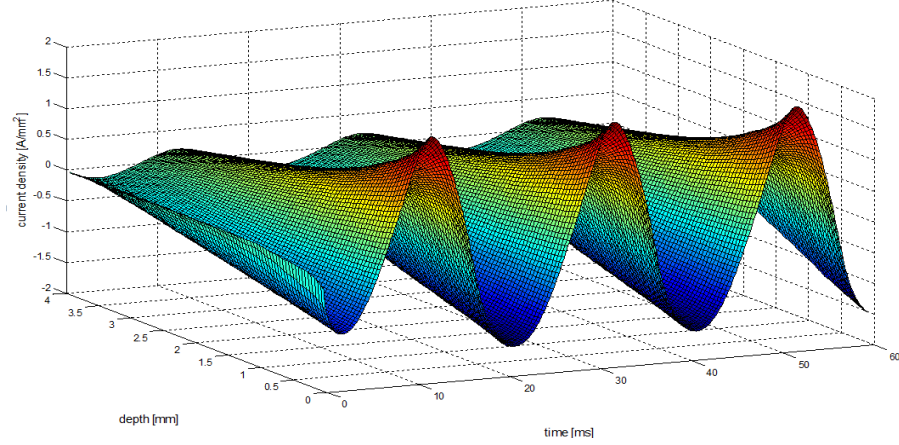


*Figure 4.1 Eddy Current density distributions with 2D second order mesh model*

The graphical results explain the eddy current behavior under skin effect. After solving Maxwell equation in section 2.2 of chapter 2, all the vectors will decrease as we move away from the coil. The decrease in the field is more rapid in the case of higher frequency, permeability and higher conductivities. This can be understood from an analytical expression given below (Popović *et. al.* 2000).

$$J_x(z) = J_x(0)e^{-z/h}e^{-zj/h} \quad (4.6)$$

Where,  $J_x(0)$  is amplitude of conductivity at zero depth and  $h$  is the penetration depth defined in equation (2.8). So as we go away from the surface closer to coil, the current density reduces exponentially. It must be noted the above analytical equation doesn't consider saturation in the material. This factor has considerable impact on the current density distribution. The complete derivation of equation (4.6) is available in the Appendix V.

The results with 3D first order and second order mesh models in Elmer are shown in figure 4.2 and figure 4.3 respectively.

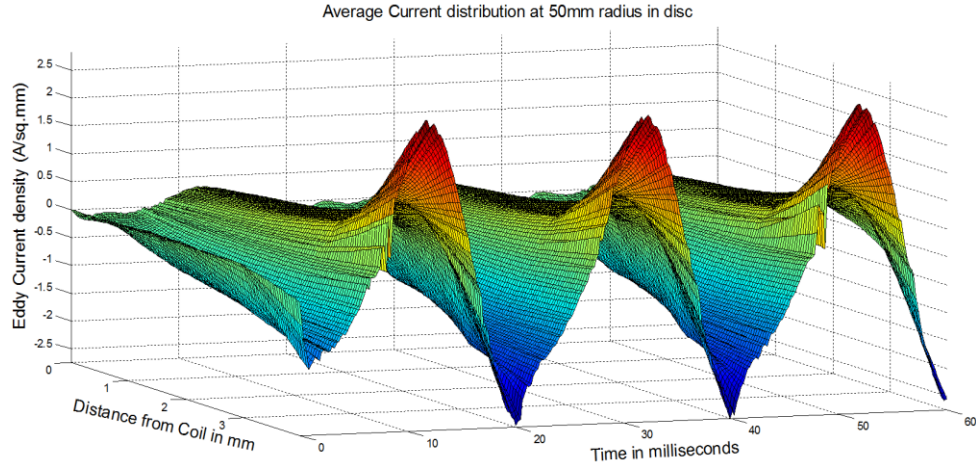


Figure 4.2 Eddy Current density distribution with 3D first order mesh model

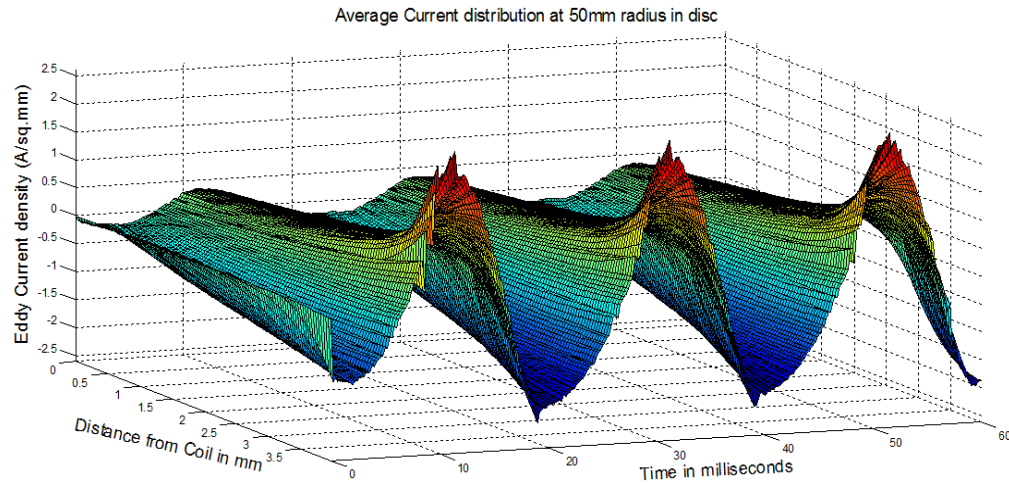
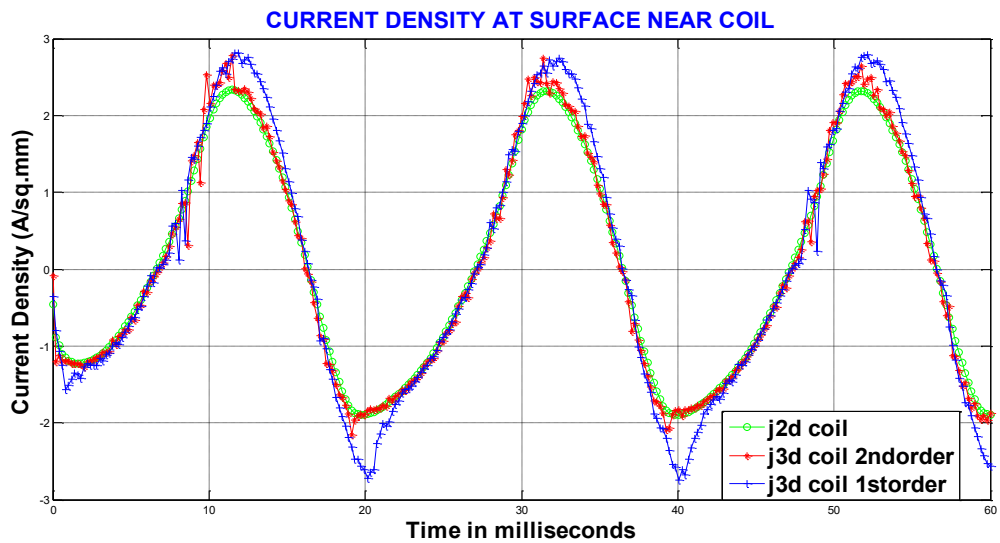


Figure 4.3 Eddy Current density distribution with 3D second order mesh model

As such, the results obtained with Elmer show the same pattern of variation except for unusual ripples. This was only observed in the case of parallel computation. The possible reason for these stays hidden behind the Elmer. However, the results for the mesh with lower element density were also analyzed by the author with serial computation. In the later, a smooth variation was obtained for the same results as shown in Appendix III.

In the above results it is difficult to visually understand how close the values are compared to the reference solution. For a better understanding, the eddy currents are compared at the outer and inner surfaces of the disc in figure 4.4 and figure 4.5.



*Figure 4.4 Comparison of eddy current density at the surface infinitely closer close to coil for FEM simulations with 2D mesh, 3D first order mesh and 3D second order mesh models*

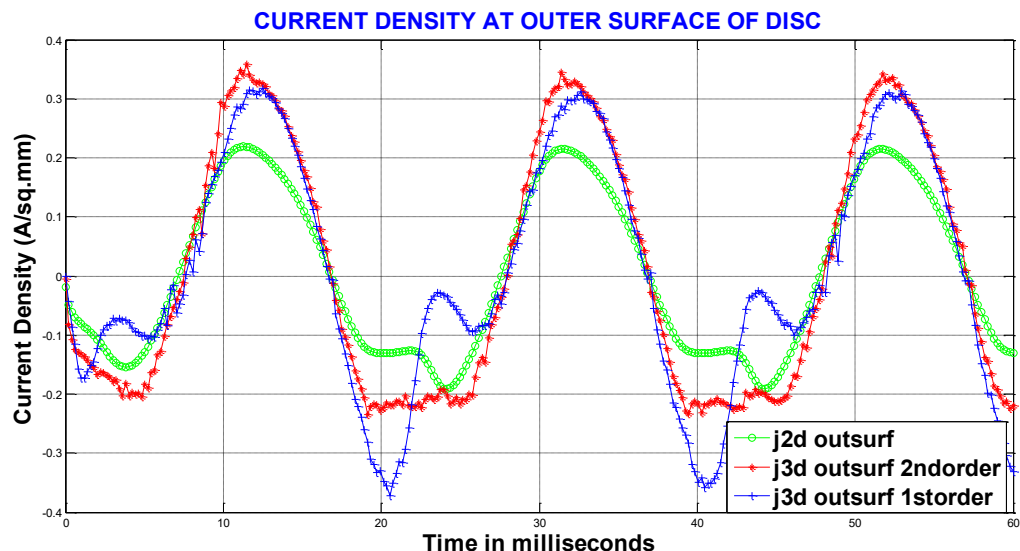


*Figure 4.5 Comparison of eddy current density at outer surface of disc for FEM simulations with 2D mesh, 3D first order mesh and 3D second order mesh models*

The current densities in both cases of three dimensional simulations have shown identical results. As per figure 4.4 both are closely following the 2D results except near the peaks. The peak values for the first order 3D results have little higher value. On the other hand, the second order mesh results are superimposed over the reference wave. In the subsequent figure, the results are plotted for the outer disc surface. It is difficult to say which is closer to the reference, as drastic variations are observed in both cases.

For further investigation of the field distribution, the flux density over the same path in the disc is measured. The values obtained in the reference case for 3 cycles are shown in figure 4.6.

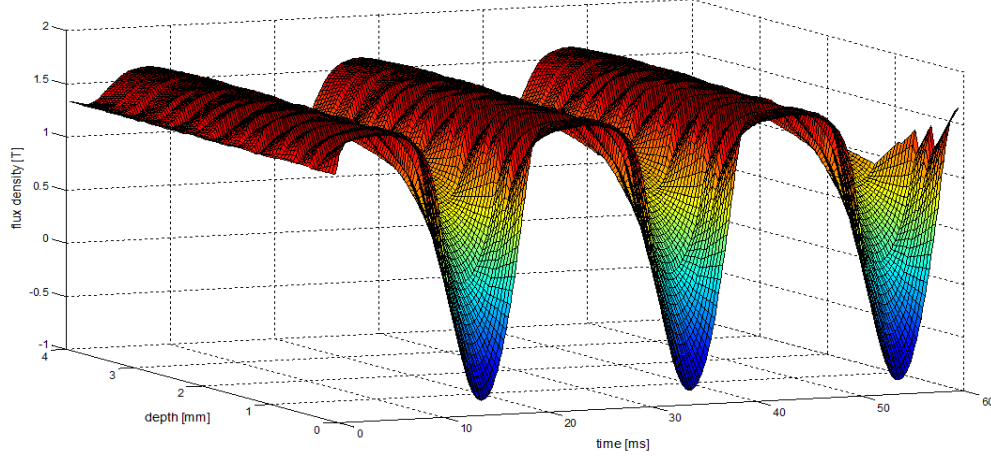


*Figure 4.6 Flux density distributions with 2D second order mesh model*

The flux density distribution behaves in the same way like the current density under the effect of the skin effect. The amplitude of the flux density closer to the surface of the coil is high and it exponentially decreases as we move farther. This distribution of flux density can also be realized with a similar expression like (4.6).

$$B_y(z) = B_y(0)e^{-z/h}e^{-zj/h} \quad (4.7)$$

Where,  $B_y(0)$  is the flux density amplitude in iron path at zero depth and  $h$  is the depth of penetration defined in equation (2.8). The background of above expression can be found in Appendix V.

The similar evaluation like in case of eddy current density is also made for flux density in first and second order meshes. The graphical results are respectively shown in figures 4.7 and 4.8.

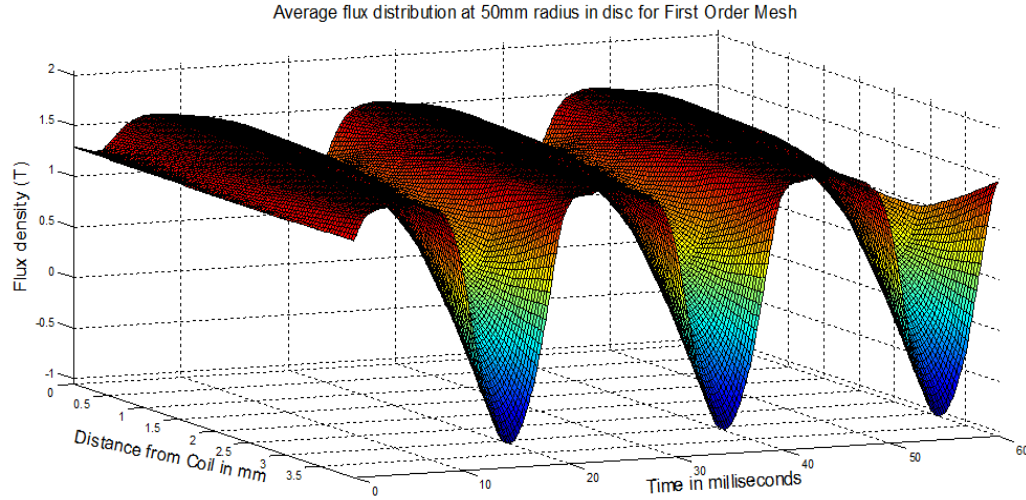


Figure 4.7 Flux density distribution with 3D first order mesh model

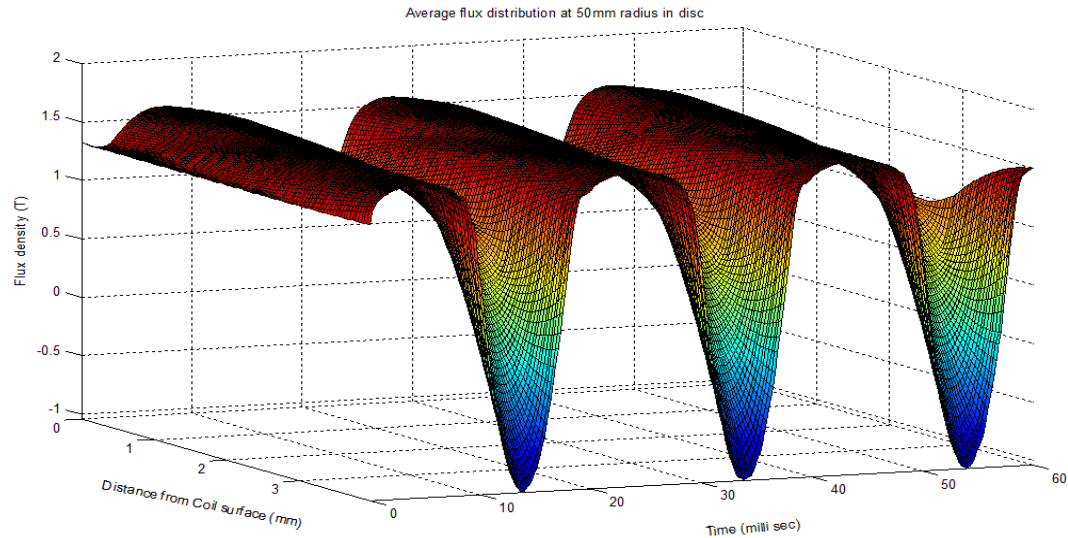
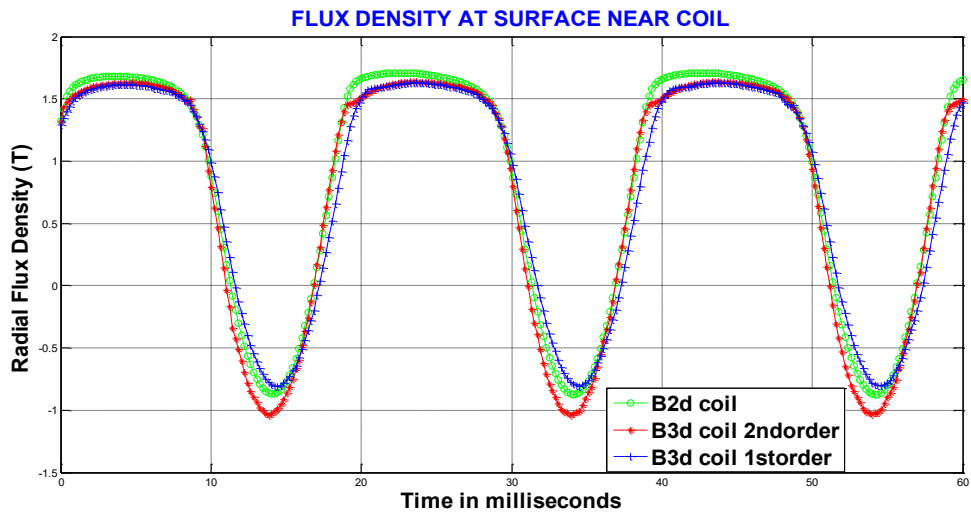
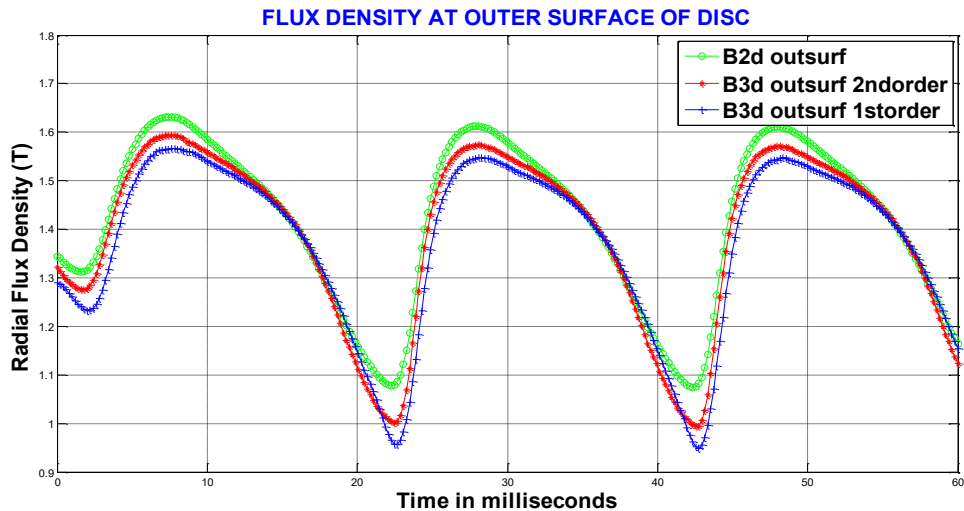


Figure 4.8 Flux density distributions with 3D second order mesh model

The flux density variation in both cases has followed the reference results. However, the skin effect is precisely captured with the second order elements when we observe the graph over the axis of distance. For a better insight, the results were again compared at the inner and outer surface of the disc. The related results for the surface infinitely close to coil are shown in figure 4.9 and the flux density at the outer surface is shown in figure 4.10. The flux densities at the surface closer to coil in both simulation cases are very close to the reference case. A little difference can be marked near the negative peak. The first order mesh provides under estimated flux density while the second order mesh has comparatively over estimated values. The scenario at the outer surface is different, as the magnitudes obtained from both simulations are less comparable to the reference.



*Figure 4.9 Comparison of flux density at disc surface infinitely closer to coil for FEM simulations with 2D mesh, 3D first order mesh and 3D second order mesh models*



*Figure 4.10 Comparison of flux density at outer surface of disc for FEM simulations with 2D mesh, 3D first order mesh and 3D second order mesh models*

#### 4.3.2 Magnetic Force evaluation with Elmer simulations

The magnetic force in bearing has a net component in the z-direction (along shaft axis). This is achieved with the design of magnetic circuit and orientation of the magnetic field. The direction of force can be well understood from the figure 4.13. The vectors in red are the magnitude of magnetic force directed along z-direction.

The forces in a 2D case were evaluated with the principle of Arkkio's method. For the comparison, the forces in 3D are computed with the Generalized nodal force (GNF) approach in the Elmer software. This method was recently implemented in the Elmer by joint efforts of Aalto University and CSC team. To get the value of total force, the nodal forces are summed over by integration over a closed domain of the shaft body. The process is carried out within Elmer itself.

The results of 3D simulations, for both mesh types are plotted along with a reference case in figure 4.11. Both, the first order and the second order meshes provide the results which obey same behavior like reference. However, the forces obtained with the second order mesh are more close to reference. This can be well understood from figure 4.12. The figure shows the evaluated percentage difference for both cases at each time instant with respect to the reference case.

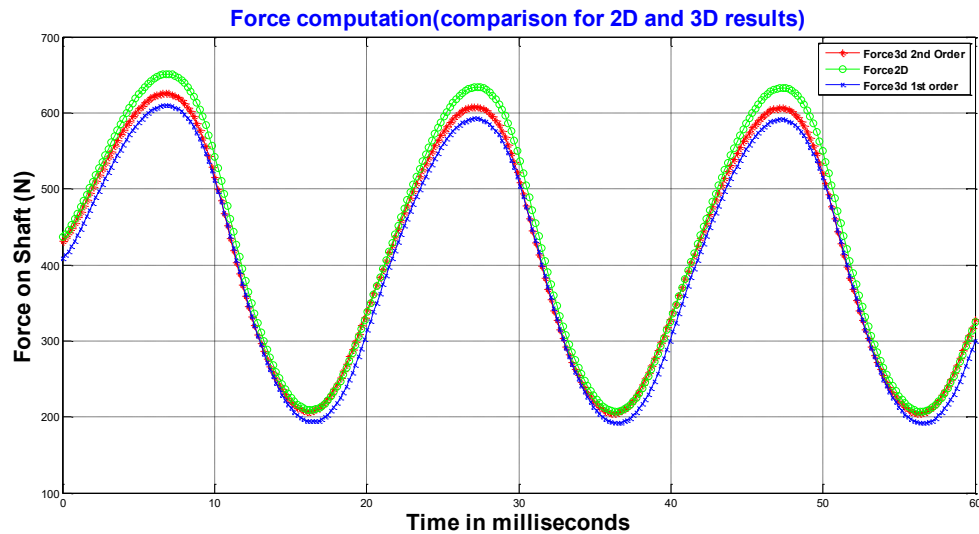


*Figure 4.11 Comparative force results with sinusoidal current excitation.*

The obtained steady state force for the first order mesh is 407.02 N and 427.78 N for the second order mesh. In the reference case 436.93 N is the obtained value for total force on the body. The solutions of steady state are the starting points for the respective time-step simulations under sinusoidal excitation. There is still some transient effect observed in the first positive peak of all three cases. Hence for comparison, third cycle is most favorable choice. The peak force magnitude in the case of reference solution is 633.14 N, while for the 3D first order and second order mesh the respective values are 592 N and 607 N. The first order mesh simulation has considerably underestimated results. However, in both case, the maximum difference is observed near peaks.

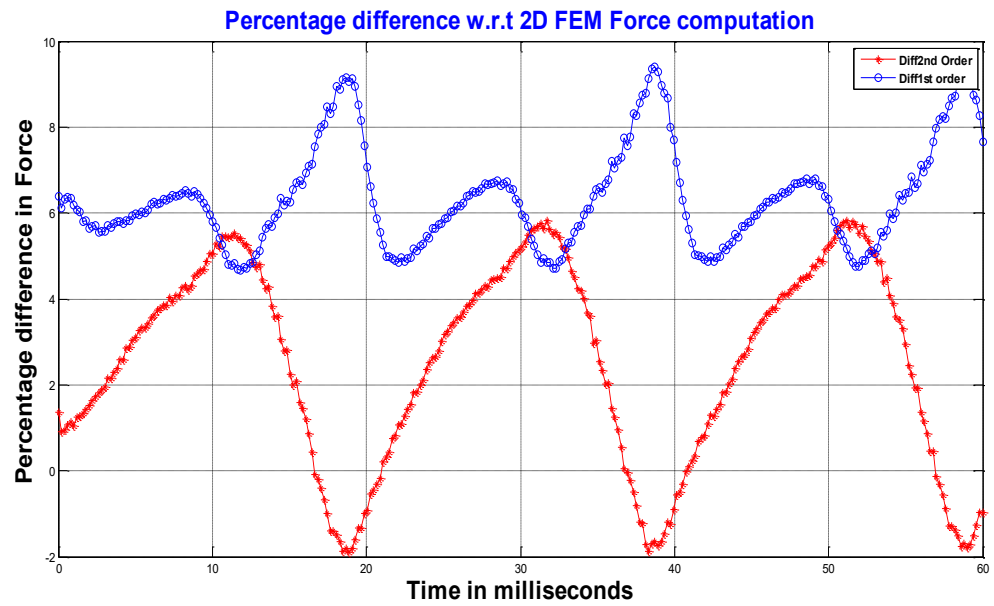


Figure 4.12 Percentage difference in Force results for 3D FEM with respect to 2D FEM

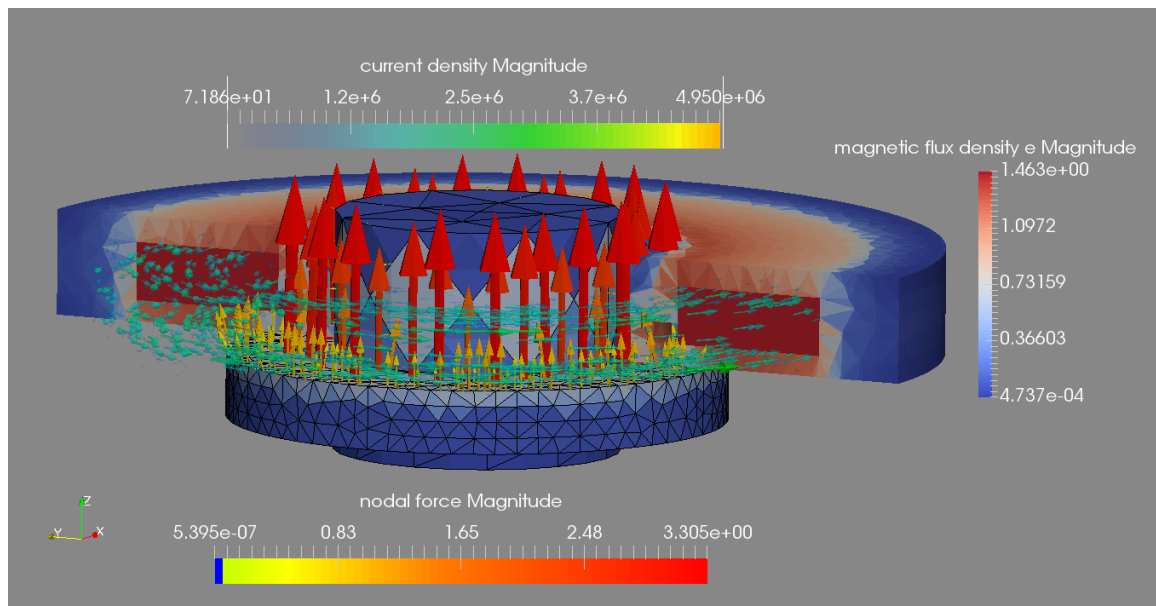


Figure 4.13 Visualization of Flux Density, Eddy current density and nodal force vector in Paraview

### 4.3.3 Eddy Current Loss and Paraview Results

The eddy current losses are calculated for the three cycles. For avoiding transient effect, the average over third cycle is considered for the loss evaluation.

The total loss evaluated in each case is shown in table 4.1.

*Table 4.1: Simulated eddy current losses in different cases:*

Model	Air (W)	Disc (W)	yoke (W)	Shaft (W)	Total Loss (W)	Percentage Difference From 2D case
<b>2D</b>	0	4.099 7	6.683	0.5503	12.369	
<b>3D (with sec. order elements)</b>					13.12	6.072 %
<b>3D (with first order elements)</b>					13.746	11.133 %

The total eddy current loss in 3D second order mesh case is 13.12 W, which is 0.728 W higher than reference values. On the other hand, simulated losses for first order mesh are higher by 1.354 W. However by adding more elements in yoke and disc for later case, the values can get closer to reference results.

### 4.3.4 Simulation Time

For achieving the goal of thesis, two categories of simulations were carried out in the Elmer software. The magnetic force, the eddy current power and the flux density distribution are computed with one simulation. The second simulation is carried out to accurately compute flux density and eddy current density distribution in the disc. Both simulations are made for 3D first order and second order mesh models. The time taken by each computation is tabulated below.

*Table 4.2: Simulation time:*

	Mesh With First order Element (360 partitions)	Mesh With Second Order Element (360 partitions)
<b>Force, Eddy current Power and Flux density in air gap</b>	177min 42sec	1711min 28sec
<b>Eddy current and Flux density values at 50mm radius</b>	601min 55sec	3880min 31sec

It can be easily seen the second order mesh case is computationally very expensive. The time taken by eddy current simulation is 3880 min and 31sec which is the longest simulation. Both meshes consist of 2,497,481 elements which call for heavy computation resources. Hence, the CSC super computer is used for all above simulations. The problem domain is divided in 360 partitions, which are then simulated with the parallel computation technique.

#### 4.4 MODIFIED DESIGN

In the axial actuator, the yoke has maximum loss according to table 4.1. The losses can be reduced by modification in design. The modification is with an idea of the breaking the path of eddy currents by not hindering actually operation of actuator. This goal can be achieved by providing radial cut in yoke section as shown in figure 4.14.



*Figure 4.14 Picture of AXB55 Actuator with radial cut in Yoke.*

The losses reduction can also be achieved by making an additional cut in disc or by introducing two or three cuts in yoke. However, the yoke with single cut is considered for analysis in current work of thesis.

The presence of cut in the magnetic circuit incurs very diligent consideration for eddy current direction. As seen from the figure 4.13, the eddy currents (with green glyph vectors) follow single direction in magnetic circuit and make a closed loop. The cut in the geometry forces the current to have second direction. This can be proven with the fundamental fact that the current flow has to be a closed loop.

Looking at the radial component of flux density in the yoke, the induced eddy current will be in cylindrical plane oriented in z direction. The component of flux density along z-direction induces current in x-y plane. This phenomenon can be very well understood from the work of Kucera et al. (1996) where he explains different configuration of cylindrical plates. The plates are excited by time varying magnetic fields in a particular direction. The proposed eddy current directions in two places of yoke are marked in figure 4.15. The red vectors are designating flux density direction.

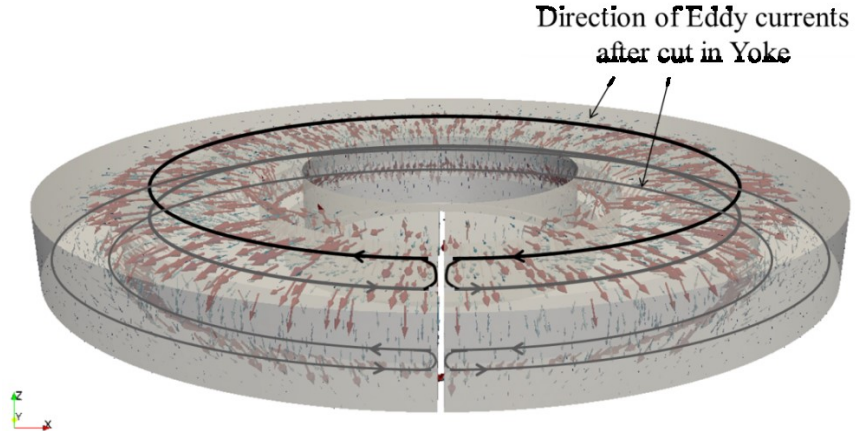


*Figure 4.15 Expected Current directions in yoke of AXB after providing radial cut.*

To obtain corresponding results, the FEM simulations are carried out using Elmer FEM software. However, the results obtained are not as expected. The constraint of time left the modified model unsolved. Since the results obtained don't make any relevance for study, they are kept out from the thesis.

#### 4.5 MODELING OF THE SHAFT ROTATION

Till now shaft is considered in stationary position without any rotational movement. In real scenario shaft of the bearing is rotating. The analysis considering rotation can be made by using Lorentz Velocity term in field or use of Mortar condition (involves mesh deformation). For the analysis in the present model the use of Lorentz velocity term is explored. The velocity term is used for prescribing velocity of moving domain. The advantage of using this approach is, no actual rotation of domain is required and hence moving mesh interface.

The introduced term, "Lorentz Velocity" is nothing but a definition of velocity vector field imposed on a medium. The name "Lorentz" is there because it is the velocity term appearing in the Lorentz force equation (Molenaar, 2000):

$$\mathbf{F} = q(\mathbf{E} + \mathbf{v} \times \mathbf{B}) \quad (4.8)$$

where  $v$  is the velocity of point charge  $q$ . In the above equation,  $\mathbf{E}$  and  $\mathbf{B}$  are the electric field strength and magnetic flux density due to moving charge  $q$ .

In the AMB model, the velocity term is used to prescribe the velocity of shaft body. The additional 'body force' defining angular velocity is required in the code of Appendix IV.

The angular velocity  $\omega$  is defined for the shaft body. For evaluation, Elmer makes use of velocity vector  $v$ , given by (Zec, 2013)

$$v = \omega \times r \quad (4.9)$$

Here ' $r$ ' is the position vector.

For evaluation of the eddy current, an additional velocity term is used along with the source term (in the equation (2.37)) (Zec, 2013).

$$\nabla \times \left( \frac{1}{\mu} \nabla \times A \right) = -\sigma \left( \frac{\partial A}{\partial t} - \nabla V - v \times \nabla \times A \right) + J_s \quad (4.10)$$

This approach however has some constraints before its application. It is only successful if the moving domain doesn't have bounded extents in the direction of motion. The domain should maintain the same physics in the direction of movement. The method also fails if the moving body contains any magnetizing source. The fact is supported by property of the Lorentz term which doesn't include part of magnetic flux induced by the motion of source. Hence the distribution of induced current in the moving domain is same and maintains uniform motion (Zec, 2013).

In the present model above method was unsuccessfully checked in Elmer software. Hence the results are not presented in this work of thesis.

# CHAPTER 5

## CONCLUSION AND DISCUSSION

This section of thesis summarizes the work by highlighting key facts about obtained results. The accuracy and time of simulation are also discussed.

From the referred literatures for thesis work, it has been observed the study of magnetic bearing requires knowledge from different spheres. This makes the magnetic bearing a wide field for research.

The purpose of the work was to build up a method for three dimensional finite element analysis of axial active magnetic bearing actuator. The task was limited to electromagnetic analysis in Elmer FEM software tool. The results are analysed with the two types of mesh element viz. the first order and the second order element. For the comparison, simulated results from the two dimensional solution are considered as the base. The model obeys axial symmetry, so it can be accurately modeled with 2D FEM. However, the idea was to analyse the complete actuator, which can also be later useful in the study of asymmetric model. As a part of work objective the realistic method is established using Elmer. For better insight and proper validation of work, simulations are carried out for first order and second order mesh. The obtained results show good agreement with reference solution. In the present model, the simulations are made current driven by defining the current density vectors in the coil geometry. The transients in the system were also dealt at initial phase. As the system holds a low time constant the transients at the start of excitation were observed to vanish after four periods. However to avoid its major effect and save some computation time, the system is first solved with DC steady state current. The obtained results were stored at some location, which are then used as starting point for time stepped simulation. The results obtained with such approach only show minor effect of transient in first two cycles and the steady state is reached right after second period. Thus we get here relaxation of one cycle. In the computed case, for achieving high accuracy enormously dense mesh is analysed and that too with the second order elements. The advantage of using DC steady state can be understood from the table of computation time in chapter 4. If DC steady state solution approach was not used then durations of each simulation would have been 1.5 times higher.

During the work phase, there was simultaneous development was being carried out in the Elmer FEM tool. The post processing solver in the Elmer has shown some abnormal pattern of results in the case of parallel computation. However, the reason is unseen and due to constraint of time author had to stay satisfied with obtained results.

In the model, some section of the yoke and disc face high gradients in the flux density and the eddy current density. In order to obtain high accuracy in the evaluation, relatively dense mesh is used in those portions. The skin depth calculation and mesh element size play important role over here. There were challenges faced for obtaining an accurate mesh element size for specific location with the use of GMSH meshing tool. However, for the consider mesh parameters in current work, the obtained total eddy current loss and eddy current are close to respective values of 2D solution. It should be noted for the higher frequencies of input current, this consideration is more critical.

The force computation is another essential feature to be considered in study of AMB. The evaluation of steady state force and the magnetic forces under high amplitude input current signal are studied through finite element analysis. The generalized nodal force approach is used in the computation and the accuracy of method was seen by closeness of the results with respect to the reference solution. The mesh density also played important role in the evaluation of forces, especially in the air gaps between the stator and the rotor section.

In comparison to the reference case, the losses in the actuator with 3D FEM simulations have respectively shown over estimation of 6.072 % and 11.133 % for the second order and the first order mesh cases. On the other hand, the force computation has been under estimated by maximum difference of 5% and 9% in same chronology. These errors are acceptable when we compare 3D and 2D FEM cases. The factors like computation method used in software, convergence of iteration, mesh element type, size of far field boundary etc. also impact the field solutions. The accuracy of obtained results can only be claimed if the measurements are done. The practical effect of stress on magnetizing property of core material also influences the magnetic force. The study of such characteristics requires and measurement requires lot of time, hence they stayed out of scope. In the presented work only single valued BH curve is considered for both 3D and 2D simulation.

# **CHAPTER 6**

## **FUTURE WORK**

The complete analysis of axial magnetic bearing incurs many aspects. However, the research work was limited to certain extent for master's thesis. In the presented model, only high amplitude simulation is touched, but a magnetic bearing also requires analysis of small signal. This is useful in design the control for predicting the forces, current, voltage and the displacement. The Elmer is expected to have this feature in near future and could be experimented in AXB55 model. The modified design is still unsolved in the current version of Elmer. The work can be taken to next step as 3D FEM method is already verified and same strategy can be used further in analysis of such asymmetries. The method of using velocity term in Elmer was explored by author and it was noticed the results were not as expected. The work in coordination with Elmer software team can resolve this issue. Considering the second order element case the computation can be very expensive of bigger models. The work of reducing the transients in time stepped simulation can be taken up in future. It will be possible to analyze same results in even less number of cycles if the initialization for time stepped simulation is accurate. Last but not the least it will be interesting to see the accuracy of results by comparing them with real measurements.

# APPENDIX I

## MAGNETIZING PROPERTY

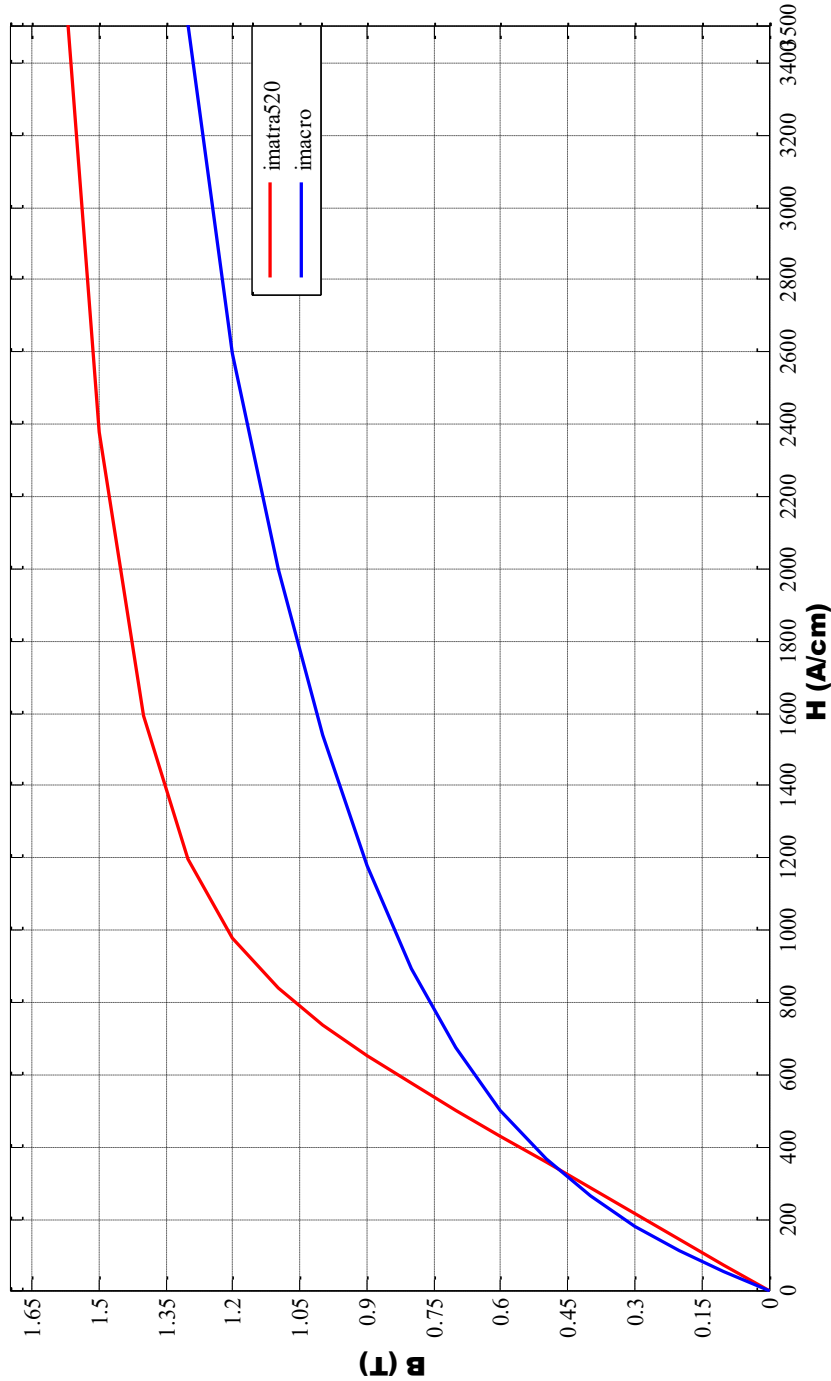


Figure 1 Material data for Imacro steel and Imatra520 steel

## APPENDIX II

### GEOMETRY DETAILS FOR AXB55

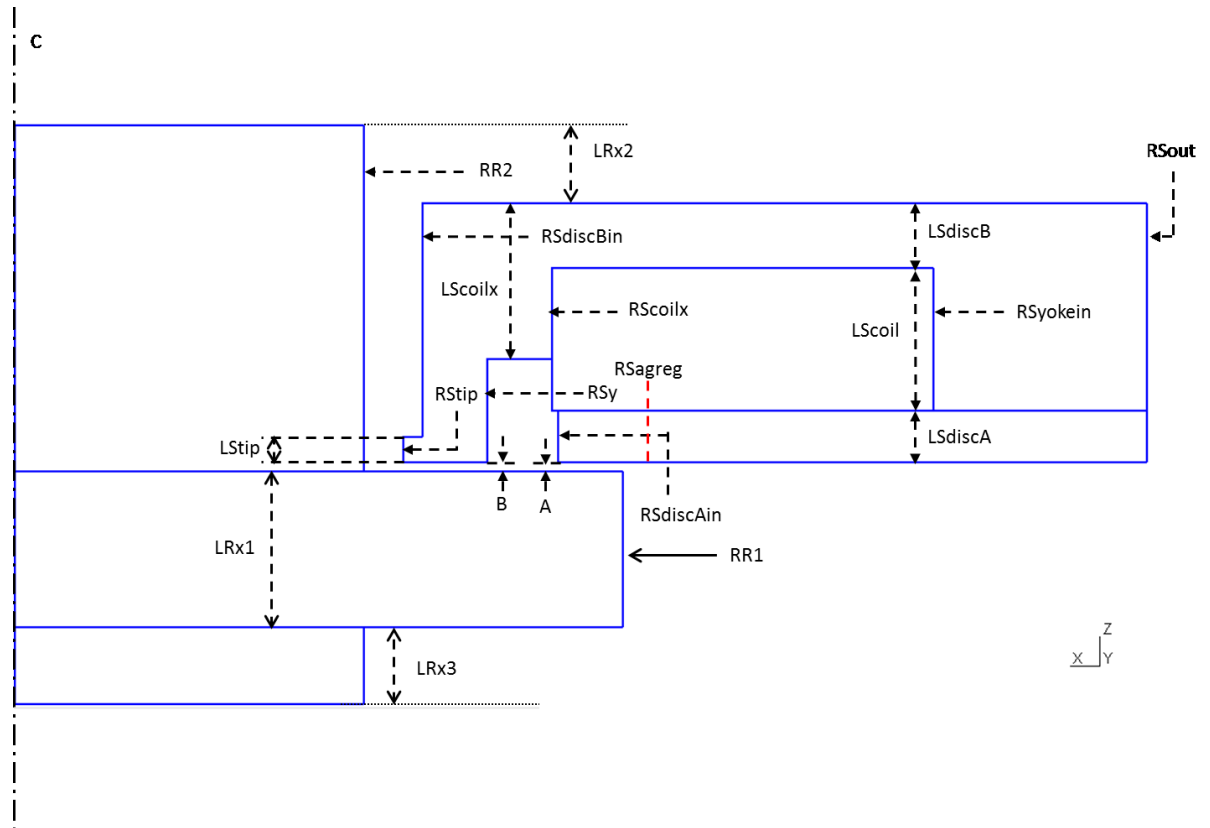


Figure 1 Cross sectional view of AXB 55 model

#### 1. Axial actuator Dimensions in m

'RSout' = 175/2000

'RSyokein' = 142/2000

'LSdiscA' = 4E-3

'LSdiscB' = 5E-3

'LScoil' = 11E-3

'RSdiscAin' = 84/2000

'RSdiscBin' = 63/2000

'RScoilx' = 83/2000

'LScoilx' = 12E-3

'LRx1' = 12E-3

'LRx2' = 10E-3

'LRx3' = 6E-3

'RSagreg' = 94/2000+2E-3

'RR1' = 94/2000

'RR2' = 54/2000

'RSy' = 73/2000

'RStip' = 60/2000

'LStip' = 2E-3

'ag' = 0.7E-3

## 2. Modified Geometry

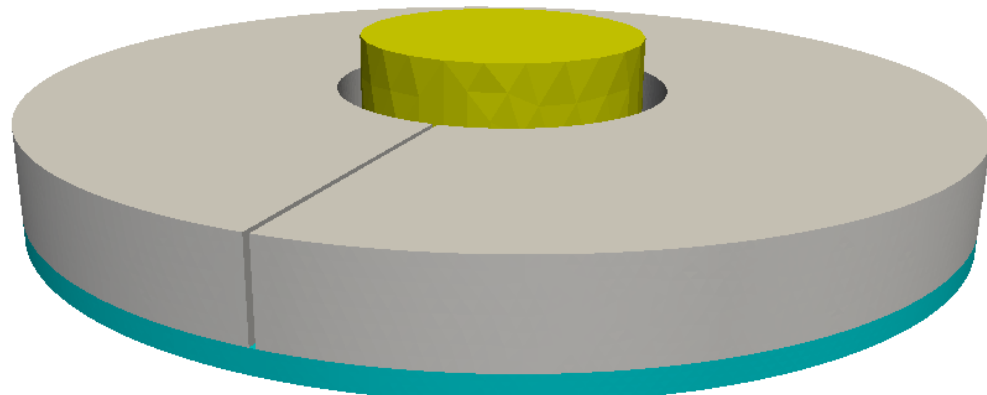


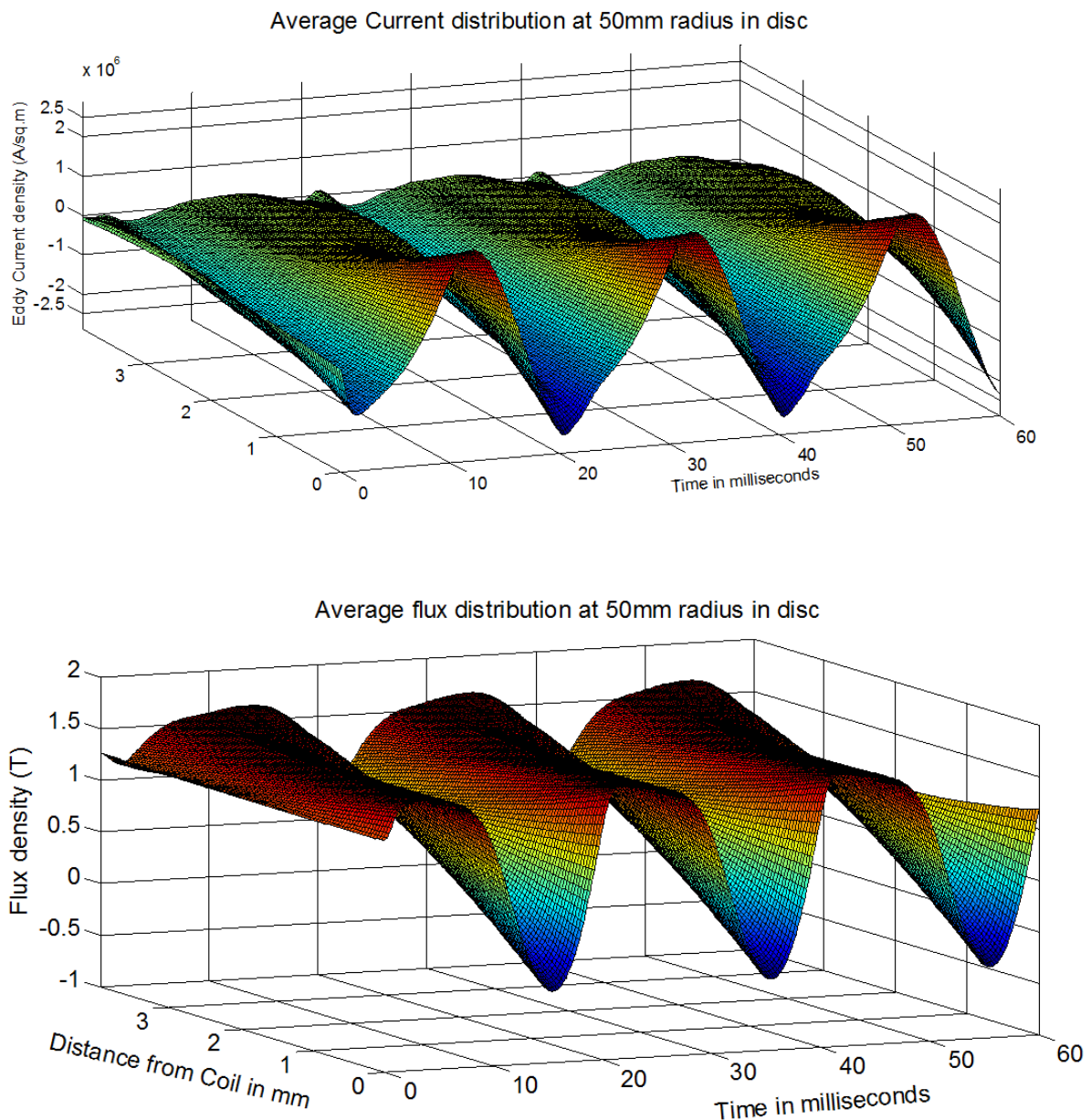
Figure 2 Geometry with 1 mm radial Cut in the Yoke

## APPENDIX III

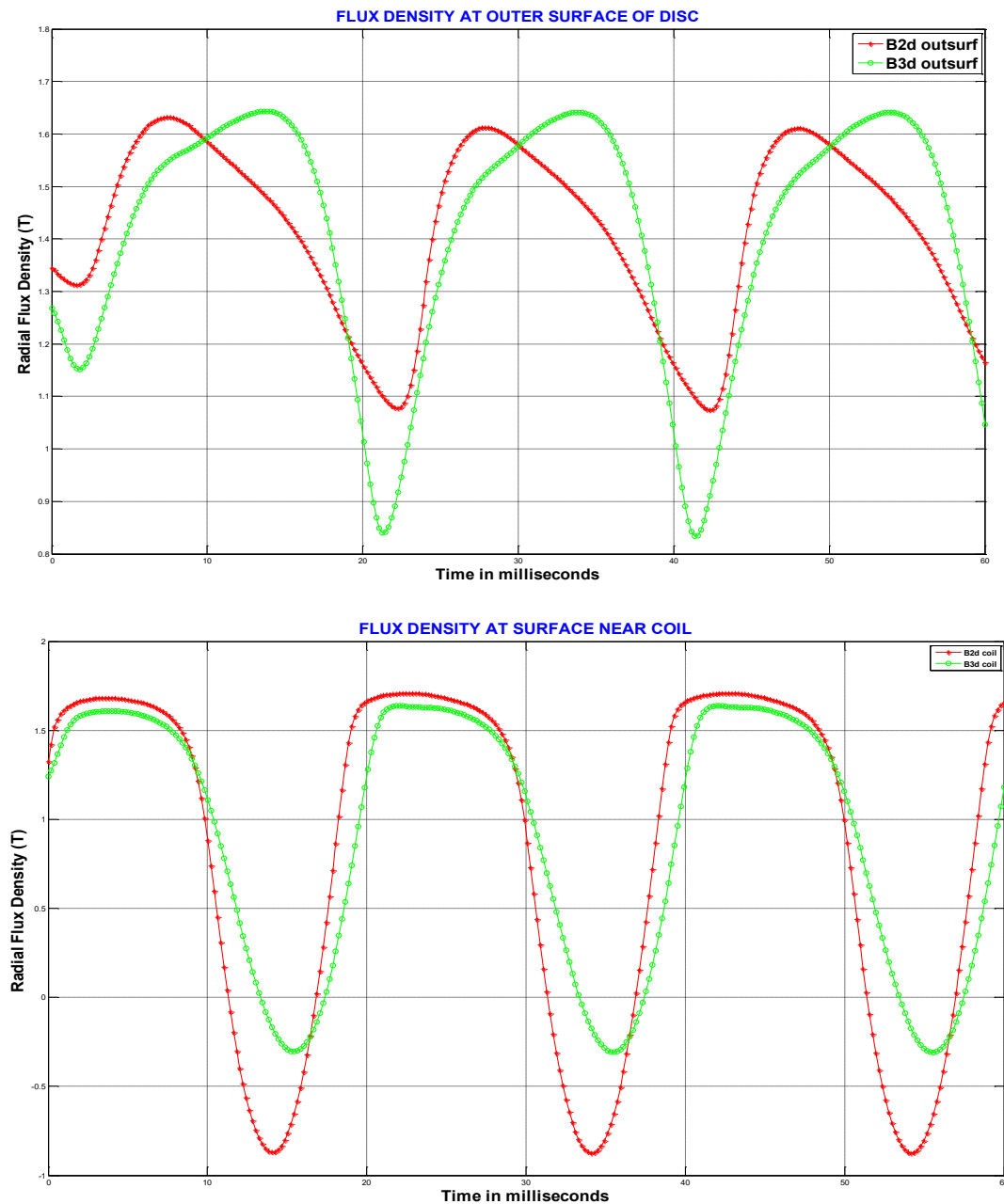
# RESULTS FOR LOWER MESH DENSITY

This appendix contains the post processed results with Serial Computation with second order elements.

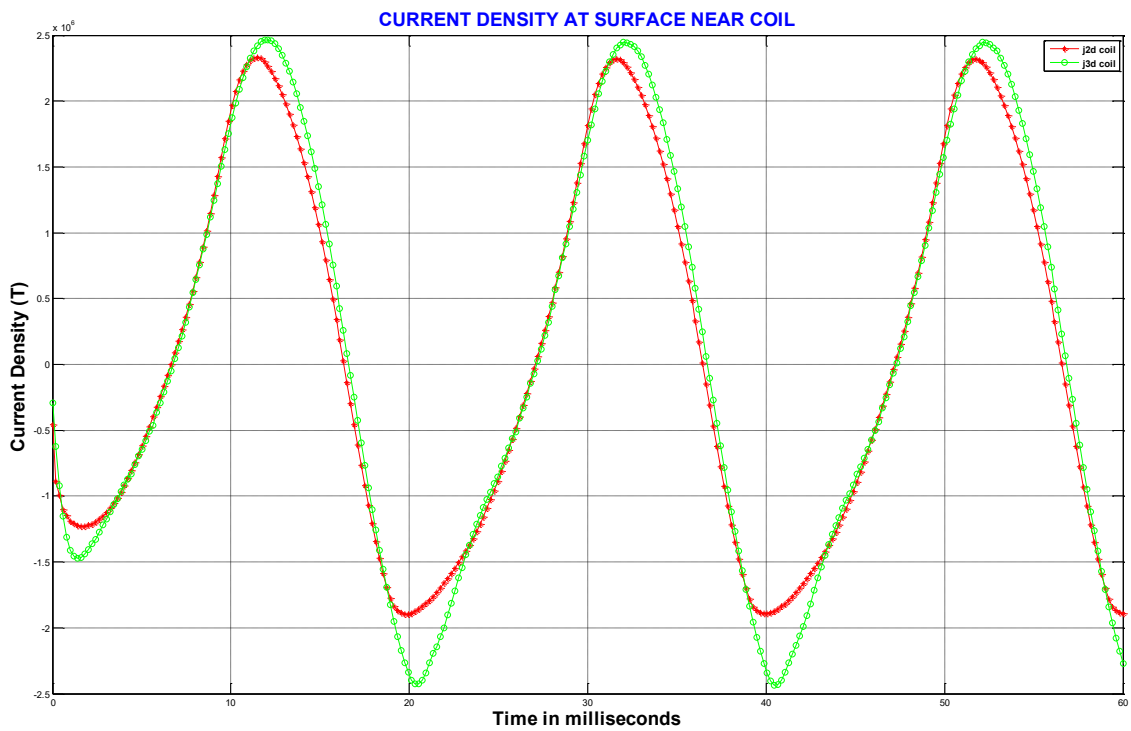
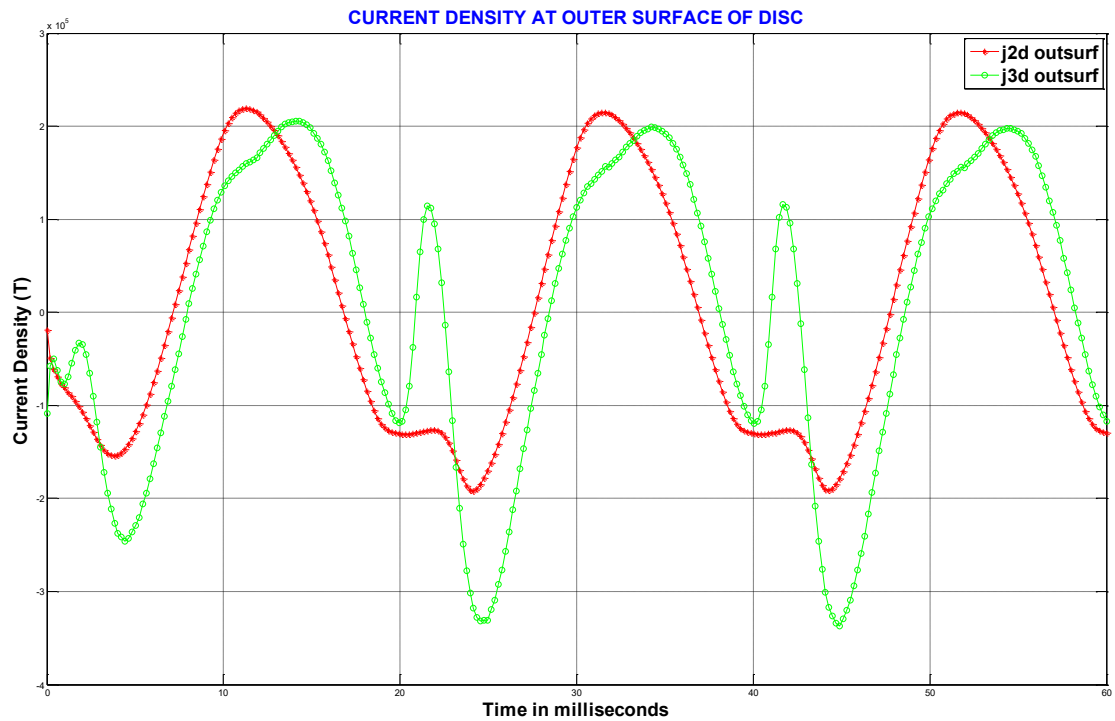
### 1. 3D Plots for simulation with mesh consisting of 64,131 second order elements



## 2. Comparison of flux densities



### 3. Comparison of current densities



# APPENDIX IV

## ELMER SIMULATION CODE

This section of appendix contains the code of Elmer Software tool which is used for obtaining the required simulation results. The code is used in file with extension ‘.sif’.

### **1. Elmer simulation code for eddy current density and flux density in disc.**

```
!Time stepped simulation for eddy current
!Parameters

$ w_coil = 314.1592654
$ j_coil = 1.1556e6
Header
    CHECK KEYWORDS "Warn"
    Mesh DB "mesh"
        Include Path ""
        Results Directory ""
End

Simulation
    Restart File = "c.result" !Start simulation from steady state
                                simulation results saved in file
                                named 'c.result'
    Max Output Level = 30
    Coordinate System = Cartesian
    Coordinate Mapping(3) = 1 2 3
    Simulation Type = Transient !Use "Steady State" for steady
                                state Simulation
    Steady State Max Iterations = 50
    Timestep Sizes = $ 1/(w_coil/(2*pi))/100
    Timestep Intervals =300
    Output Intervals = 100
    Timestepping Method = BDF
    BDF Order = 2
    Coordinate Scaling = Real 0.001
    !Post File = AMB.ep
    Output File = File t.result !Used for saving results after
                                specified time steps intervals.
    Output Global Variables = Logical True
    Simulation Time = Logical True
End

Constants
    Gravity(4) = 0 -1 0 9.82
```

```

Stefan Boltzmann = 5.67e-08
Permittivity of Vacuum = 8.8542e-12
Boltzmann Constant = 1.3807e-23
Unit Charge = 1.602e-19
End

!Solver for evaluating vector potential
Solver 1
Equation = MGDynamics
Procedure = "MagnetoDynamics" "WhitneyAVSolver"
Variable = AV
!Angular Frequency = $ w_coil
Fix Input Current density = Logical True

Newton-raphson iteration = True
Steady State Convergence Tolerance = 1.0e-3
Nonlinear System Convergence Tolerance = 1.0e-3
Nonlinear System Max Iterations = 1
Nonlinear System Newton After Iterations = 10
Nonlinear System Newton After Tolerance = 1.0e-3
Nonlinear System Relaxation Factor = 1
Use Piola Transform = True !Can be removed for first order
                           mesh element
Quadratic Approximation = Logical True !set also Piola to True
                                         for this one. Can be
                                         removed for first order
                                         mesh element

Linear System Solver = "Iterative"
Linear System Symmetric = True
Linear System Iterative Method = BiCGStab
Linear System Max Iterations = 500
Linear System Convergence Tolerance = 1.0e-8
Linear System Preconditioning = none
Linear System Residual Output = 50
Linear System Abort Not Converged = False
Linear system normwise backward error = True
!linear system GCR restart = 100
End

! This section of solver provides solution of derived fields with
! nodal approximation.

Solver 2
Equation = MGDynamicsCalc
Procedure = "MagnetoDynamics" "MagnetoDynamicsCalcFields"
Potential Variable = String "AV"

Steady State Convergence Tolerance = 1.0e-5
Nonlinear System Convergence Tolerance = 1.0e-5
Nonlinear System Max Iterations = 20
Nonlinear System Newton After Iterations = 3

```

```

Nonlinear System Newton After Tolerance = 1.0e-5
Nonlinear System Relaxation Factor = 1
Use Piola Transform = True !Can be removed for first order mesh
                           element
Quadratic Approximation = Logical True ! set also Piola to True
                                         for this one. Can be
                                         removed for first order
                                         mesh element

Linear System Solver = Iterative
Linear System Symmetric = True
Linear System Iterative Method = CG
Linear System Max Iterations = 500
Linear System Convergence Tolerance = 1.0e-7
Linear System Preconditioning = none
Linear System ILUT Tolerance = 1.0e-5
Linear System Abort Not Converged = False
Linear System Residual Output = 1
Linear System Precondition Recompute = 1
!Calculate Electric Field = True
Calculate Magnetic Field Strength = True
Calculate Current Density = True
!Calculate electric energy = Logical true
!Calculate Nodal Forces = Logical True
!Calculate Magnetic Vector Potential= True
!Calculate Maxwell Stress = Logical True

!This enforces the component reduction operator to activated
!Update Components(3) = 1 2 3
End

!Solver 3 to 6 are for defining the line with 100 points at 4
!sections of Disc, and provide solution value for each point.

Solver 3
Exec Solver = after timestep
Equation = SaveLine1
Procedure = "SaveData" "SaveLine"
Output directory = T0x-1y
Filename = a1.dat
Polyline Coordinates(2,3) = 0 -0.05 0.0227 0 -0.05 0.0187
Polyline Divisions(1) = 99 !divided above line defined line in
                           99 sections
End

Solver 4
Exec Solver = after timestep
Equation = SaveLine2
Procedure = "SaveData" "SaveLine"
Output directory =T0x1y
Filename = a2.dat

```

```

Polyline Coordinates(2,3) = 0 0.05 0.0227 0 0.05 0.0187
Polyline Divisions(1) = 99
End

Solver 5
  Exec Solver = after timestep
  Equation = SaveLine3
  Procedure = "SaveData" "SaveLine"
  Output directory = T1x0y
  Filename = a3.dat
  Polyline Coordinates(2,3) = 0.05 0 0.0227 0.05 0 0.0187
  Polyline Divisions(1) = 99
End

Solver 6
  Exec Solver = after timestep
  Equation = SaveLine4
  Procedure = "SaveData" "SaveLine"
  Output directory = T-1x0y
  Filename = a4.dat
  Polyline Coordinates(2,3) = -0.05 0 0.0227 -0.05 0 0.0187
  Polyline Divisions(1) = 99
End

Equation 1
  Name = "MGDyn"
  Active Solvers(1) = 1
End

Equation 2
  Name = "disc"
  Active Solvers(2) = 1 2
End

Material 1
  Name = "air"
  Relative Permeability = real 1
  Permittivity = 8.8542e-12
End

Material 2
  Name = "copper"
  Relative Permeability = real 1
  ! Electric Conductivity = 59e6
  Permittivity = 8.8542e-12
End

! Material property for Imacro and Imatra520 are defined based on
! single valued material curve in Appendix I.

Material 3
  Name = "imacro"

```

```

    Permittivity = 8.8542e-12
    Electric Conductivity = 4.3e6
    !Relative Permeability = real 800
    H-B Curve = Variable coupled iter
        Real Monotone Cubic
        Include HB_Imacro
    End
End

Material 4
    Name = "imatra520"
    Electric Conductivity = 4.3e6
    Permittivity = 8.8542e-12
    !Relative Permeability = real 800
    H-B Curve = Variable coupled iter
        Real Monotone Cubic
        Include HB_Imatra520
    End
End

!Current excitation equations for the model.
Body Force 1
    Name = "Current"
        ! tx(0) - x
        ! tx(1) - y
        ! tx(2) - z
        ! tx(3) - t
    Current Density 1 = Variable coordinate,time
        Real MATC "-"
        (j_coil)*(tx(1)/sqrt((tx(1)*tx(1))+(tx(0)*tx(0))))*(2+sin(w_coil*
        tx(3)))
    Current Density 2 = Variable coordinate,time
        Real MATC
        "(j_coil)*(tx(0)/sqrt((tx(1)*tx(1))+(tx(0)*tx(0))))*(2+sin(w_coil*
        tx(3)))"
    End

Body 1
    Target Bodies(1) = 1
    Name = "shaft"
    Equation = 1
    Material = 3
    !Initial condition = 1
    Shaft Force 1 = Logical True
    Shaft Force 2 = Logical True
    Shaft Force 3 = Logical True
End

Body 2
    Target Bodies(1) = 2
    Name = "yoke"
    Equation = 1

```

```

Material = 4
!Initial condition = 1
End

Body 3
Target Bodies(1) = 3
Name = "disc"
Equation = 2
Material = 4
!Initial condition = 1
End

Body 4
Target Bodies(1) = 4
Name = "coil"
Equation = 1
Material = 2
Body Force = 1
!Initial condition = 1
End

Body 5
Target Bodies(1) = 5
Name = "air"
Equation = 1
Material = 1
!Initial condition = 1
End

!Boundary condition at the outer most boundary for problem.
Boundary Condition 1
Target Boundaries(6) = 62 63 64 65 66 67
Name = "far"
AV {e} = real 0
AV = real 0
End

```

## 2. Elmer simulation code for total magnetic force and eddy current loss calculation

```

!Time stepped simulation for Force
!Parameters

$ w_coil = 314.1592654
$ j_coil = 1.1556e6

Header
  CHECK KEYWORDS "Warn"
  Mesh DB "mesh"
    Include Path ""
    Results Directory ""

```

```
End
```

```
Simulation
```

```
Restart File = "timestep2.result"!Start simulation from steady
state simulation results
saved in file named
'timestep2.result'
```

```
Max Output Level = 30
Coordinate System = Cartesian
Coordinate Mapping(3) = 1 2 3
Simulation Type = Transient !Use "Steady State" for steady
state Simulation
```

```
Steady State Max Iterations = 50
Timestep Sizes = $ 1/(w_coil/(2*pi))/100 ! delta t
Timestep Intervals =200
Output Intervals = 100
Timestepping Method = BDF
BDF Order = 2
Coordinate Scaling = Real 0.001
!Post File = AMB.ep
Output File = File timestep3.result !Used for saving results
after specified time steps
intervals.
```

```
!Output Global Variables = Logical True
```

```
End
```

```
Constants
```

```
Gravity(4) = 0 -1 0 9.82
Stefan Boltzmann = 5.67e-08
Permittivity of Vacuum = 8.8542e-12
Boltzmann Constant = 1.3807e-23
Unit Charge = 1.602e-19
```

```
End
```

```
!Solver for evaluating vector potential
```

```
Solver 1
```

```
Equation = MGDynamics
Procedure = "MagnetoDynamics" "WhitneyAVSolver"
Variable = AV
!Angular Frequency = $ w_coil
Fix Input Current density = Logical True
Newton-raphson iteration = true
Steady State Convergence Tolerance = 1.0e-5
Nonlinear System Convergence Tolerance = 1.0e-5
Nonlinear System Max Iterations = 20
Nonlinear System Newton After Iterations = 3
```

```

Nonlinear System Newton After Tolerance = 1.0e-5
Nonlinear System Relaxation Factor = 1
Use Piola Transform = Logical True
Quadratic Approximation = Logical True

!Definition of element. This is optional in current version of
!Elmer. However author recommends its use, as Elmer is seen to
!provide faster solution when element definition is provided in
!sif file. This fact requires more experimental simulaitons.

Element = "n:1 e:2 -brick b:6 -prism b:2 -quad_face b:4 -
tri_face b:2"

Linear System Solver = iterative
Linear System Symmetric = True
Linear System Iterative Method = BiCGStab
!Linear System Iterative Method = GCR
Linear System Max Iterations = 1000
Linear System Convergence Tolerance = 1.0e-9
Linear System Preconditioning = none
Linear System Residual Output = 50
Linear System Abort Not Converged = False
Linear system normwise backward error = True
!linear system GCR restart = 100
End

! This section of solver provides solution of derived fields with
! nodal approximation.

Solver 2
Equation = MGDynamicsCalc
Procedure = "MagnetoDynamics" "MagnetoDynamicsCalcFields"
Potential Variable = String "AV"

Steady State Convergence Tolerance = 1.0e-5
Nonlinear System Convergence Tolerance = 1.0e-5
Nonlinear System Max Iterations = 20
Nonlinear System Newton After Iterations = 3
Nonlinear System Newton After Tolerance = 1.0e-5
Nonlinear System Relaxation Factor = 1
Use Piola Transform = Logical True !Can be removed for first
order mesh element

Quadratic Approximation = Logical True !Set also Piola to True
for this one. Should be
removed for first order
mesh element

Linear System Solver = Iterative
Linear System Symmetric = True

```

```

Linear System Iterative Method = CG
Linear System Max Iterations = 1000
Linear System Convergence Tolerance = 1.0e-8
Linear System Preconditioning = none
Linear System ILUT Tolerance = 1.0e-5
Linear System Abort Not Converged = False
Linear System Residual Output = 1
Linear System Precondition Recompute = 1
Calculate Electric Field = True
Calculate Magnetic Field Strength = True
Calculate Current Density = True
Calculate electric energy = Logical true
Calculate Nodal Forces = Logical True ! Evaluates magnetic forces
with GNF approach.
Calculate Magnetic Vector Potential= True
!Calculate Maxwell Stress = Logical True
End

```

```

!Solver to obtain .VTU file for visualizing the field
!Solution in Paraview.

```

```

Solver 3
  Exec Solver = after timestep
  Equation = "ResultOutput"
  Procedure = "ResultOutputSolve" "ResultOutputSolver"
  Output File Name = AMB
  Vtu format = Logical True
  Ascii Output = False
  Save Geometry Ids = Logical True
  !Vector Field 1 = String Magnetic Field Strength
  !Vector Field 2 = String Magnetic Flux Density
  !Show Variables = Logical True
End

```

```

!Solver for obtaining total force on the shaft body. The output
!file obtained from this solver also provides data of total eddy
!current loss in magnetic circuit.

```

```

Solver 4
  Exec Solver = after timestep
  Equation = "bodyforce"
  Procedure = "SaveData" "SaveScalars"
  Filename = "force_transient.dat"
  Parallel Reduce = Logical True
  Variable 1 = Nodal Force 1
  Mask Name 1 = Shaft Force 1
  Operator 1 = Body Sum
  Variable 2 = Nodal Force 2
  Mask Name 2 = Shaft Force 2
  Operator 2 = Body Sum
  Variable 3 = Nodal Force 3
  Mask Name 3 = Shaft Force 3

```

```

Operator 3 = Body Sum

end

Equation 1
  Name = "MGDyn"
  Active Solvers(3) = 1 2 3
End

! Material property for Imacro and Imatra520 are defined based on
! single valued material curve in Appendix I.

Material 1
  Name = "air"
  Relative Permeability = real 1
  Permittivity = 8.8542e-12
End

Material 2
  Name = "copper"
  Relative Permeability = real 1
  ! Electric Conductivity = 59e6
  Permittivity = 8.8542e-12
End

Material 3
  Name = "imacro"
  Permittivity = 8.8542e-12
  Electric Conductivity = 4.3e6
  !Relative Permeability = real 800
  H-B Curve = Variable coupled iter
  Real Monotone Cubic
  Include HB_Imacro
End
End

Material 4
  Name = "imatra520"
  Electric Conductivity = 4.3e6
  Permittivity = 8.8542e-12
  !Relative Permeability = real 800
  H-B Curve = Variable coupled iter
  Real Monotone Cubic
  Include HB_Imatra520
End
End

!Velocity term feature for analysing rotation without using any
!moving mesh interface

!Body Force 1

```

```

!Name = "rotation"
!Angular Velocity 3 = real $ omega
!End

!Current excitation equations for the model.

Body Force 1           !It should be 'Body force 2' while using
                        velocity term feature
Name = "Current"
  ! tx(0) - x
  ! tx(1) - y
  ! tx(2) - z
  ! tx(3) - t
Current Density 1 = Variable coordinate,time
  Real MATC "-
(j_coil)*(tx(1)/sqrt((tx(1)*tx(1))+(tx(0)*tx(0))))*(2+sin(w_coil*
tx(3)))"
Current Density 2 = Variable coordinate,time
  Real MATC
"(j_coil)*(tx(0)/sqrt((tx(1)*tx(1))+(tx(0)*tx(0))))*(2+sin(w_coil*
tx(3)))"
End

Body 1
  Target Bodies(1) = 1
  Name = "shaft"
  Equation = 1
  Material = 3
  !Initial condition = 1
  Shaft Force 1 = Logical True
  Shaft Force 2 = Logical True
  Shaft Force 3 = Logical True

End

Body 2
  Target Bodies(1) = 2
  Name = "yoke"
  Equation = 1
  Material = 4
  !Initial condition = 1
  !yoke Force 1 = Logical True
  !yoke Force 2 = Logical True
  !yoke Force 3 = Logical True
End

Body 3
  Target Bodies(1) = 3
  Name = "disc"
  Equation = 1
  Material = 4
  !Initial condition = 1

```

```

!disc Force 1 = Logical True
!disc Force 2 = Logical True
!disc Force 3 = Logical True
End
Body 4
  Target Bodies(1) = 4
  Name = "coil"
  Equation = 1
  Material = 2
  Body Force = 1
  !Initial condition = 1
End

Body 5
  Target Bodies(1) = 5
  Name = "air"
  Equation = 1
  Material = 1
  !Initial condition = 1
End

!Boundary condition at the outer most boundary for problem.

Boundary Condition 1
  Target Boundaries(6) = 62 63 64 65 66 67
  Name = "far"
  AV {e} = real 0
  AV = real 0
End

```

# APPENDIX V

## PENETRATION DEPTH

This appendix provides basic derivation of analytical expression for current density and flux density behavior under skin effect.

From the equations 2.10 and 2.12 in chapter 2, we have

$$\nabla \times \mathbf{H} = \mathbf{J} \quad \nabla \times \mathbf{E} = -\frac{\partial \mathbf{B}}{\partial t}$$

In the frequency domain

$$\nabla \times \mathbf{E} = -j\omega \mathbf{B} \quad (1)$$

The relation between current density and flux density can be easily extended from the above equation.

$$\nabla \times \mathbf{J} = -j\omega \sigma \mathbf{B} \quad (2)$$

$$\nabla \times \mathbf{B} = \mu \mathbf{J} \quad (3)$$

In the presented results, the x-component of the current density ( $J_x$ ) and the y-component of the flux density ( $B_y$ ) are observed. The coordinate directions are mentioned with reference to figure 3.1. Both  $J_x$  and  $B_y$  are seen to be affected over the  $z$  direction. Hence we will use ordinary differential equation here and the relations in (2) and (3) can be represented as

$$\frac{dJ_x}{dz} = -j\omega \sigma B_y \quad (4)$$

$$\frac{dB_y}{dz} = \mu J_x \quad (5)$$

By differentiating expression (4) with respect to  $z$  and making the use of relation (5) we obtain

$$\frac{d^2 J_x}{dz^2} = j\omega \mu \sigma J_x \quad (6)$$

The solution of above differential equation has a simple form

$$J_x(z) = J_1 e^{qz} + J_2 e^{-qz} \quad (7)$$

Where

$$q = \sqrt{j\omega\mu\sigma} = \sqrt{j} * \sqrt{\omega\mu\sigma} = (1+j) * \sqrt{\frac{\omega\mu\sigma}{2}} \quad (8)$$

From equation (3.1)

$$q = (1+j) * \frac{1}{h} \quad (9)$$

Hence,

$$J_x(z) = J_1 e^{z(1+j)/h} + J_2 e^{-z(1+j)/h} \quad (10)$$

By substituting  $z = 0$ , the current density becomes  $J_x(0)$  while inserting  $z = \infty$  makes current to rise indefinitely which is not possible. This leaves us with an option to put  $J_1=0$  and hence the equation can be rewritten as

$$J_x(z) = J_x(0) e^{-z/h} e^{-zj/h} \quad (11)$$

So as we go away from the surface closer to coil, the current density reduces exponentially.

The equation (11) can be represented in terms of  $B_y$  when substitution is made for  $J_x$ .

$$\frac{d^2 B_y}{dz^2} = j\omega\mu\sigma B_y \quad (12)$$

By following the same process derivation, we end up with the expression of  $B_y$  as function of the distance in z-direction.

$$B_y(z) = B_y(0) e^{-z/h} e^{-zj/h} \quad (13)$$

So now it can be seen that the flux density also shows an exponential reduction as we move far from the disc surface near the coil.

## REFERENCES

- Antila M., “Electromechanical Properties of Radial Magnetic Bearings” 1998
- Arkkio A., 1987, “Analysis of induction motors based on the numerical solution of the magnetic field and circuit equations,” ISBN 951-22-6076-X.
- Bastos J. P. A., 2003, “Electromagnetic Modeling by Finite Element Methods”, ISBN 0203911172, 9780203911174.
- Belahcen A., 2004, “Magnetoelasticity, Magnetic Forces and Magnetostriction in Electrical Machines” Doctoral Thesis, Helsinki University of Technology.
- Bergot M., Durufle M., 2011, “High-Order Optimal Edge Elements for Pyramids, Prisms and Hexahedra”
- Betschon F., 2000, “Design Principles of Integrated Magnetic Bearings” Dipl. El.-Ing. ETH
- Biro O., 1990, “finite element analysis of 3-d eddy currents”, IEEE Transc. Magnetics Vol 26,
- Biro O., Preis K., and Ticar I., 2005, “A FEM method for eddy current analysis in laminated media,” COMPEL: Int. J. for Compu. Math. Elect. Electron. Eng., ISSN: 0332-1649, vol. 24 Iss. 1, pp. 241–248.
- Biro O., 1999, “Edge element formulations of eddy current problems,” Comput. Methods in Appl. M., vol. 169, no. 3-4, pp. 391–405.
- Bossavit A., 1989, “Simplicial Finite Elements for Scattering problems in Electromagnetism”, Computational Methods Appl. Mech. And Eng., Vol. 76, pp. 299-316
- Bossavit A., 1992, “Edge-element Computation of the Force Field In Deformable Bodies”, IEEE Transaction on Magnetics, Vol. 28, No. 2, March 1992, pp. 1263-1266.
- Carmignani C., Forte P., Rustighi E., 2001, “ Active control of rotor vibrations by means of Piezoelectric actuator” Proceedings of DETC’01
- Coulomb J. L. 1983, “A Methodology for the Determination of Global Electromechanical Quantities from a Finite Element Analysis and its Application to the Evaluation of Magnetic Forces, Torques and Stiffness”, IEEE Transactions on Magnetics, Vol. MAG-19, No. 6, November 1983, pp. 2514–2519.
- Gouws R., 2004, “The development of an axial active magnetic bearing”
- Hull J. R., “Low Rotational Drag in high-temperature superconducting bearing” IEEE transaction, 1995

J.L. Coulomb, 1983, "A methodology for the determination of global quantities from a finite element analysis and its application to the evaluation of magnetic forces, torques and stiffness", IEEE Transactions on Magnetics MAG-19, pp. 2514-2519, No.6.

Kameari, A. 1993, "Local Calculation of Forces in 3D FEM with edge elements", International Journal of Applied Electromagnetics in Materials, Vol. 3, 1993, pp. 231–240.

Kataja J., Belahcen A., Sathayan S. 2015, "Generalized Nodal Forces in Elmer and other new features in MagnetoDynamicsCalcFields"

Knospe C., Fittro R, Stephens L. S., "Control of a high speed machining spindle via mu-synthesis", Conference: Control Applications, Proceedings of the 1997 IEEE International Conference , PP: 912-917.

Kucera L., Ahrens M., 1996, "A model for Axial Magnetic Bearings Including Eddy Currents", 1996, NASA Conference Publication 3336, pp.421-436.

Lantto E., 1999 , "Robust Control of Magnetic Bearing in Subcritical Bearing"

Larsonneur Rene "Design and Control of Active Magnetic Bearing Systems for High Speed Rotation" 1990 Dissertation ETH Zurich

Luomi J.,1993 'Finite Element Methods for Electrical Machines', Lect. Notes, Chalmers University of Technology

Maslen, E.; Hermann, P.; Scott, M.; Humphris, R. R., 1993, "Practical limits to the performance of magnetic bearings: Peak force, slew rate, and displacement sensitivity", NASA. Langley Research Center, Magnetic Suspension Technology Workshop; p 273-286.

Mason J. L.,1982, "Finite Element Solution for Electromagnetic scattering from two dimensional bodies"

Mayergoys I.D., Abdel-Kader F.M., September 1984, "The analytical calculation of eddy-current losses in steel laminations subjected to rotating magnetic fields" IEEE Transactions on Magnetics, Vol. MAG-20, No. 5, pp. 2007-2009.

Meeker D. C., Filatov A. V., "Effect of Magnetic Hysteresis on Rotation Losses in Heteropolar Magnetic Bearing", IEEE Transaction, 2004

Meunier G., 2010, "The Finite Element Method for electromagnetic Modeling", John Wiley & Sons

Molenaar L., 2000, "A novel Planar Magnetic Bearing and Motor Configuration applied in a Positioning Stage", Delft University of Technology, the Netherlands.

Popescu M., 2007, "On the Physical Basis of Power Losses in Laminated Steel and Minimum-Effort Modeling in an Industrial Design Environment", Industry Applications Conference, 2007. 42nd IAS Annual ing. IEEE Conference Record.

Popović Z. B., Popović B. D., "Introductory Electromagnetics", Prentice Hall, 2000, ISBN 0201326787, 9780201326789

Preis K., Bardi I., Biro O., Magele C., Renhart W., Richter K.R. and Vrisk G., 1991, "Numerical analysis of 3D magnetostatic fields", IEEE Transactions on Magnetics 27, 3798-3803.

Pyrhonen J., Jokinen T., Hrabovcova V., "Design of Rotating Electrical Machines", John Wiley & Sons.

Råback P., Malinen M., Ruokolainen J., Pursula A., Zwinger T., 2016, "Elmer Models Manual", CSC – IT Center for Science.

Ruokolainen J., Malinen M., Råback P., Zwinger T., Pursula A., Byckling M., 2016, "Elmer Solver Manual", CSC – IT Center for Science.

Reddy C. J., Deshpade M. D., Cockrell C. R. and Bech F. B., 1994, "Finite Element Method for Eigenvalue Problems in Electromagnetics", NASA Technical paper 3485.

Renhart W., Stögner H. and Preis K., 1988, "Calculation of 3D eddy current problems by finite element method using either an electric or a magnetic vector potential", IEEE Transactions on Magnetics (Volume:24 , Issue: 1 ), pp. 122 – 125

Sadowski N., 1996, "Dynamic Modeling of a Newly Designed Linear Actuator using 3D Edge Elements Analysis", IEEE Transactions on Magnetics Vol 32 NO.3, pp.1633-1636.  
Schweitzer G., 2002, " Active Magnetic Bearing- Chances and Limitations" Proc. 6th Internat. IFToMM Conf. on Rotor Dynamics, Sydney

Schweitzer G., Maslen E. H., 2009 "Magnetic Bearings Theory, Design, and Application to Rotating Machinery" ISBN 978-3-642-00496-4.

TommilaV., 2002, "Aksiaalisen magneettilaakerin magneettipiirin malli"

Webb J. P., 1993, "Edge elements and what they can do for you," IEEE Transactions on Magnetics., vol. 29, no. 2, pp. 1460–1465.

Yang C. and knopse C., 1997 , "Optimal Control of a Magnetic Bearing without Bias Flux"

Zec M., 2013, "Theory and Numerical Modelling of Lorentz Force Eddy Current Testing", Fakultät für Elektrotechnik und Informationstechnik der Technischen Universität Ilmenau